Article

Immunity

Expansion of T memory stem cells with superior anti-tumor immunity by Urolithin A-induced mitophagy

Graphical abstract

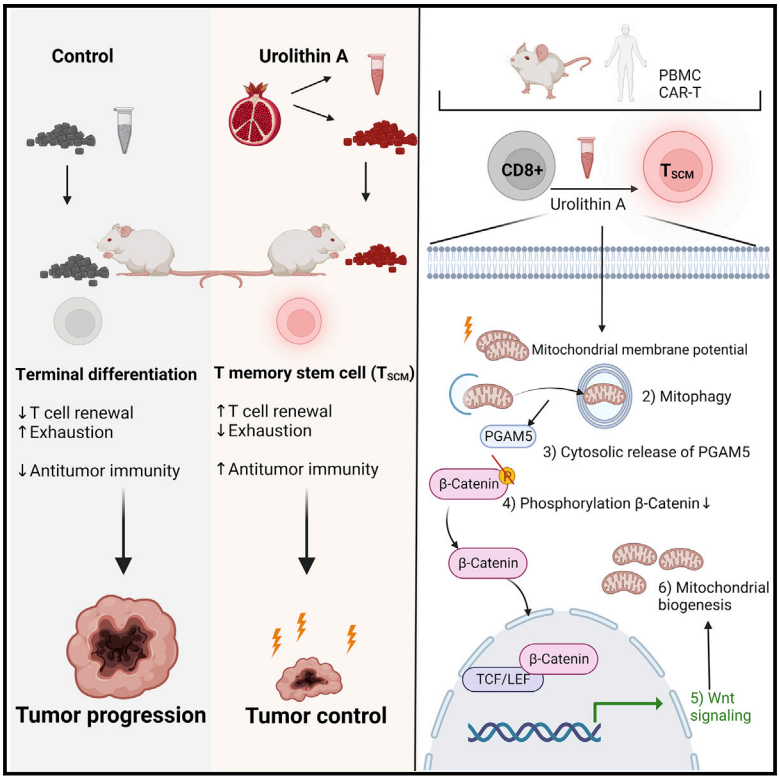

Highlights

- UA induces Pink1-dependent mitophagy in $CD8^+$ cells causing PGAM5 release
- Cytosolic PGAM5 augments Wnt signaling to drive T_{SCM} formation
- T_{SCM} induction augments anti-tumor immunity *in vivo*
- Urolithin can be used for *ex vivo* expansion of CAR-expressing T_{SCM}

Authors

Dominic Denk, Valentina Petrocelli, Claire Conche, ..., Pénélope A. Andreux, Chris Rinsch, Florian R. Greten

Correspondence

greten@gsh.uni-frankfurt.de

In brief

Anti-tumor immunity is limited by reduced T cell persistence and antigen presentation. Denk et al. show that Urolithin A, a natural metabolite of pomegranate extract, enhances antigen presentation in cancer and promotes mitophagy in $CD8^+$ T cells, resulting in generation regenerative stem cell-like memory (T_{SCM}) cells with enhanced anti-tumor properties.

Denk et al., 2022, Immunity *55*, 2059–2073
November 8, 2022
https://doi.org/10.1016/j.immuni.2022.09.014

CellPress

Immunity

CellPress
OPEN ACCESS

Article

Expansion of T memory stem cells with superior anti-tumor immunity by Urolithin A-induced mitophagy

Dominic Denk,[1,2] Valentina Petrocelli,[1] Claire Conche,[1] Moritz Drachsler,[2] Paul K. Ziegler,[3] Angela Braun,[4,5] Alena Kress,[1] Adele M. Nicolas,[1,6] Kathleen Mohs,[1] Christoph Becker,[7,8] Markus F. Neurath,[7,8] Henner F. Farin,[1,5,6] Christian J. Buchholz,[4,5] Pénélope A. Andreux,[9] Chris Rinsch,[9] and Florian R. Greten[1,5,6,10,*]

[1]Institute for Tumor Biology and Experimental Therapy, Georg-Speyer-Haus, 60596 Frankfurt/Main, Germany
[2]Department of Medicine 1, Goethe-University Hospital Frankfurt, Frankfurt/Main, Germany
[3]Dr. Senckenberg Institute of Pathology, University Hospital Frankfurt, Frankfurt/Main, Germany
[4]Molecular Biotechnology and Gene Therapy, Paul-Ehrlich Institut, Langen, Germany
[5]German Cancer Consortium (DKTK) and German Cancer Research Center (DKFZ), 69120 Heidelberg, Germany
[6]Frankfurt Cancer Institute, Goethe University Frankfurt, 60596 Frankfurt/Main, Germany
[7]Department of Medicine 1, Friedrich-Alexander-Universität Erlangen-Nürnberg (FAU), 91054 Erlangen, Germany
[8]Deutsches Zentrum Immuntherapie (DZI), 91054 Erlangen, Germany
[9]Amazentis SA, EPFL Innovation Park, Lausanne, Switzerland
[10]Lead contact
*Correspondence: greten@gsh.uni-frankfurt.de
https://doi.org/10.1016/j.immuni.2022.09.014

SUMMARY

T memory stem cells (T_{SCM}) display increased self-renewal and prolonged survival capabilities, thus preventing T cell exhaustion and promoting effective anti-tumor T cell responses. T_{SCM} cells can be expanded by Urolithin A (UA), which is produced by the commensal gut microbiome from foods rich in ellagitannins and is known to improve mitochondrial health. Oral UA administration to tumor-bearing mice conferred strong anti-tumor $CD8^+$ T cell immunity, whereas *ex vivo* UA pre-treated T cells displayed improved anti-tumor function upon adoptive cell transfer. UA-induced T_{SCM} formation depended on Pink1-mediated mitophagy triggering cytosolic release of the mitochondrial phosphatase Pgam5. Cytosolic Pgam5 dephosphorylated β-catenin, which drove Wnt signaling and compensatory mitochondrial biogenesis. Collectively, we unravel a critical signaling pathway linking mitophagy to T_{SCM} formation and suggest that the well-tolerated metabolic compound UA represents an attractive option to improve immune therapy.

INTRODUCTION

Colorectal cancer (CRC) is the third-most diagnosed cancer worldwide, and its mortality remains high, especially in advanced stages (Sung et al., 2021). CRC progression strongly depends on its complex tumor microenvironment (TME) (Schmitt and Greten, 2021). The particular importance of T cells for CRC prognosis is well exemplified by the development of an immmunoscore (Pagès et al., 2018) that assesses the density of cytotoxic $CD8^+$ cells in the tumor. The local immunoscore can predict patient survival in CRC patients with metastases (van den Eynde et al., 2018). However, CRC comprises a clear unresolved paradox, as only microsatellite instable (MSI^+) CRCs have been demonstrated to adequately respond to immune checkpoint blockade so far (Le et al., 2015). Successful strategies to reliably sensitize microsatellite stable (MSS) colorectal tumors to immune therapy are lacking.

We have shown that mitophagy in intestinal epithelial cells (IECs) in mice with an IEC-restricted Stat3 deletion ($Stat3^{\Delta IEC}$) increases antigen presentation, thereby enhancing $CD8^+$ T cell-dependent anti-tumor immunity during early intestinal tumorigenesis (Ziegler et al., 2018). However, apart from proper antigen presentation, efficacy of immunotherapy is limited by T cell exclusion from the TME or T cell exhaustion (Chen and Mellman, 2017). The TME confers T cell exhaustion by structurally and metabolically modifying T cells via chronic signaling cues (Scharping et al., 2016). Among the many pathways driving changes in T cell phenotype and function, mitochondrial dynamics have been described to alter $CD8^+$ T cell fate (Buck et al., 2016). In particular, effector tumor-infiltrating lymphocytes (TILs) in the TME display decreased mitophagy, resulting in terminal exhaustion driven by accumulation of depolarized mitochondria (Yu et al., 2020b). Therefore, enhancing T cell fitness in the TME by promoting mitophagy represents an attractive goal for cancer therapy, considering the potentially positive effect of mitophagy in both IEC and T cells. However, currently, no clinically feasible methods of inducing mitophagy for cancer treatment are available.

Urolithin A (UA) is a natural metabolite of elagitannins, of which pomegranates present a main source (Espín et al., 2013). Metabolization of elagitannins into UA depends on the appropriate gut microbiome. However, alterations in the microbiome that occur with age lead to limited production of UA, such that the aging population produces less than half of the UA produced by younger individuals (Cortés-Martín et al., 2018). Studies utilizing concentrated forms of UA suggest that dietary supplementation induces mitophagy *in vivo*, slowing the progression of aging-related diseases (reviewed in D'Amico et al., 2021). Rodents fed with a UA-high diet display superior muscle function and recovery of muscle function in mice with Duchenne muscular dystrophy (Luan et al., 2021). In *C. elegans*, UA confers higher mitochondrial content and prolonged lifespan (Ryu et al., 2016). Moreover, UA has immunomodulatory effects in monocytic cells that drive attenuation of inflammation in various tissues (Toney et al., 2021) and an impact on adaptive immunity by expanding FoxP3$^+$ T regulatory cells (Ghosh et al., 2021) or blocking Th1/Th17 cell infiltration in a model of EAE (Shen et al., 2021). In humans, commercially available supplements containing UA have been deemed safe with a favorable bioavailability profile (Andreux et al., 2019). As the accumulation of mitochondria is a characteristic of exhausted, dysfunction TIL (Yu et al., 2020b), we hypothesized that induction of mitophagy via UA might constitute a way of augmenting anti-tumor immunity. Here, we explored the effects of UA in colorectal carcinogenesis and demonstrate that UA induces MHC-I upregulation on tumor epithelia and promotes expansion of T memory stem cells (T_{SCM}), thus strongly inducing a protective anti-tumor CD8$^+$ T cell immunity.

RESULTS

Urolithin A suppresses intestinal tumor growth in a T cell-dependent manner

To examine whether UA-dependent mitophagy mimicked the effect of *Stat3*$^{\Delta IEC}$ mice (Ziegler et al., 2018) and prevented intestinal tumor development in a T cell-dependent manner, we employed a model of azoxymethane (AOM)-induced tumorigenesis. FVB mice were injected with the procarcinogen AOM once a week for 6 weeks and kept for 18 weeks on an UA-containing diet (2.28 g/kg) or control diet (Figure 1A). Oral UA administration led to a significant decrease in tumor incidence and tumor size (Figures 1B–1D). This was accompanied by an increased infiltration of CD3$^+$ T cells into the colonic mucosa (Figures 1E and 1F). To confirm UA-induced mitophagy and to explore whether UA could be employed therapeutically in more advanced CRC, we took advantage of a recently developed tumor organoid system (Nicolas et al., 2022). We treated APTK organoids (characterized by loss of *Apc*, *Trp53*, and *Tgfbr2* as well as expression of oncogenic Kras^{G12D}) for 48 h with increasing concentrations of UA (Figure 1G) and observed a dose-dependent formation of lysosomes (Figure 1H; Figure S1A) and a concomitant loss of MitoTracker staining (Figure 1I; Figure S1A). This was paralleled by a marked upregulation of MHC-I (Figure 1J) validating our previous observation linking mitophagy in IEC to MHC-I upregulation (Ziegler et al., 2018). To examine the therapeutic potential of UA, we subcutaneously (s.c.) transplanted APTK organoids into C57BL/6 mice (Figure 1K). Tumor-bearing mice were subsequently subjected to the UA-supplemented diet, which resulted in significantly reduced tumor growth and enhanced CD8$^+$ T cell infiltration (Figures 1L–1N). When we transplanted APTK organoids s.c. into *Rag1*$^{-/-}$ mice, the absence of mature T and B cells abrogated the protective effect of UA (Figure 1O). Similarly, depletion of CD8$^+$ T cells led to exacerbated tumor growth in both control and UA-fed cohorts (Figures 1P and 1Q), confirming that UA-induced tumor suppression was T cell dependent. Consequently, we confirmed that UA sensitized APTK tumors to PD-1 (programmed cell death protein 1) blockade, although immune checkpoint inhibition alone did not affect APTK-tumor growth (Figures 1R and 1S).

UA promotes T_{SCM} differentiation

Mitochondrial remodeling is associated with alterations in T cell fate (Buck et al., 2016; Yu et al., 2020b). Given the observed dependency of the UA effect on CD8$^+$ T cells, we wondered whether UA may also directly affect T cell fate commitment. Purified T cells from FVB mice were stimulated with αCD3/αCD28 beads to induce T cell differentiation into effector T cell subsets in the presence or absence of UA for up to 72 h (Figure 2A). UA administration blocked differentiation into effector T cells (Figures 2B and 2C) and resulted in a significant increase of naive CD44^{lo}CD62L^{hi} T cells (Figures S1B and S1C). In addition, we observed a reduction of central memory cells (T_{CM}), whereas the frequency of effector memory cells (T_{EM}) remained unaltered (Figures S1D and S1E). In CD4$^+$ cells, we only observed changes at later time points, characterized by less naive-like CD4$^+$ cells, but enhanced frequency of T_{EM} cells (Figures S1F–S1H). Previously, a rare naive-like subset of T cells with enhanced stemness capabilities, termed T_{SCM} has been identified (Gattinoni et al., 2009). T_{SCM} are marked by extreme longevity, their ability to self-renew, and potential for immune reconstitution (Gattinoni et al., 2017) which translates into potent anti-tumor immunity. Phenotypically, T_{SCM} represent a subset of minimally differentiated T cells, which share a CD44^{lo}CD62L^{hi} phenotype with naive T cells, but are phenotypically distinct by expressing high levels of *Sca1* (Gattinoni et al., 2009). Indeed, UA led to a significantly increased number of these CD44$^-$CD62L$^+$Sca1^{hi} T_{SCM} (Figure 2D) that were characterized by a reduced mitochondrial membrane potential as well as increased CD95 expression (Figures 2E and 2F). On the contrary, UA did not promote enhanced T_{SCM} formation in CD4$^+$ cells (Figure S1I). Furthermore, UA treatment led to dose-dependent T cell death *in vitro* (Figures S2A and S2B) and restricted CD8$^+$ T cell division (Figures S2C and S2D). This was associated with reduced cyclin D1 expression (Figure S2E), in line with previous observations that link T_{SCM} reprogramming to halted proliferation (Gattinoni et al., 2009; Verma et al., 2021). Moreover, we observed that T_{SCM} were only formed in activated T cells (Figure S2F). Excluding the possibility that UA reduces TCR-mediated activation of T cells, thus limiting effector formation by retaining a naive-like state, we found that UA-treated T cells show equivalent phosphorylation of Stat1 (Gamero and Larner, 2000) compared with vehicle controls (Figure S2G).

In vivo, UA administration led to a marked increase of CD8$^+$CD44^{lo}CD62L^{hi}Sca1^{hi} T cells in APTK-induced tumors (Figure 2G); however, no change in CD4$^+$ T_{SCM} or in an antigen-presenting or immune-suppressing TME represented by dendritic

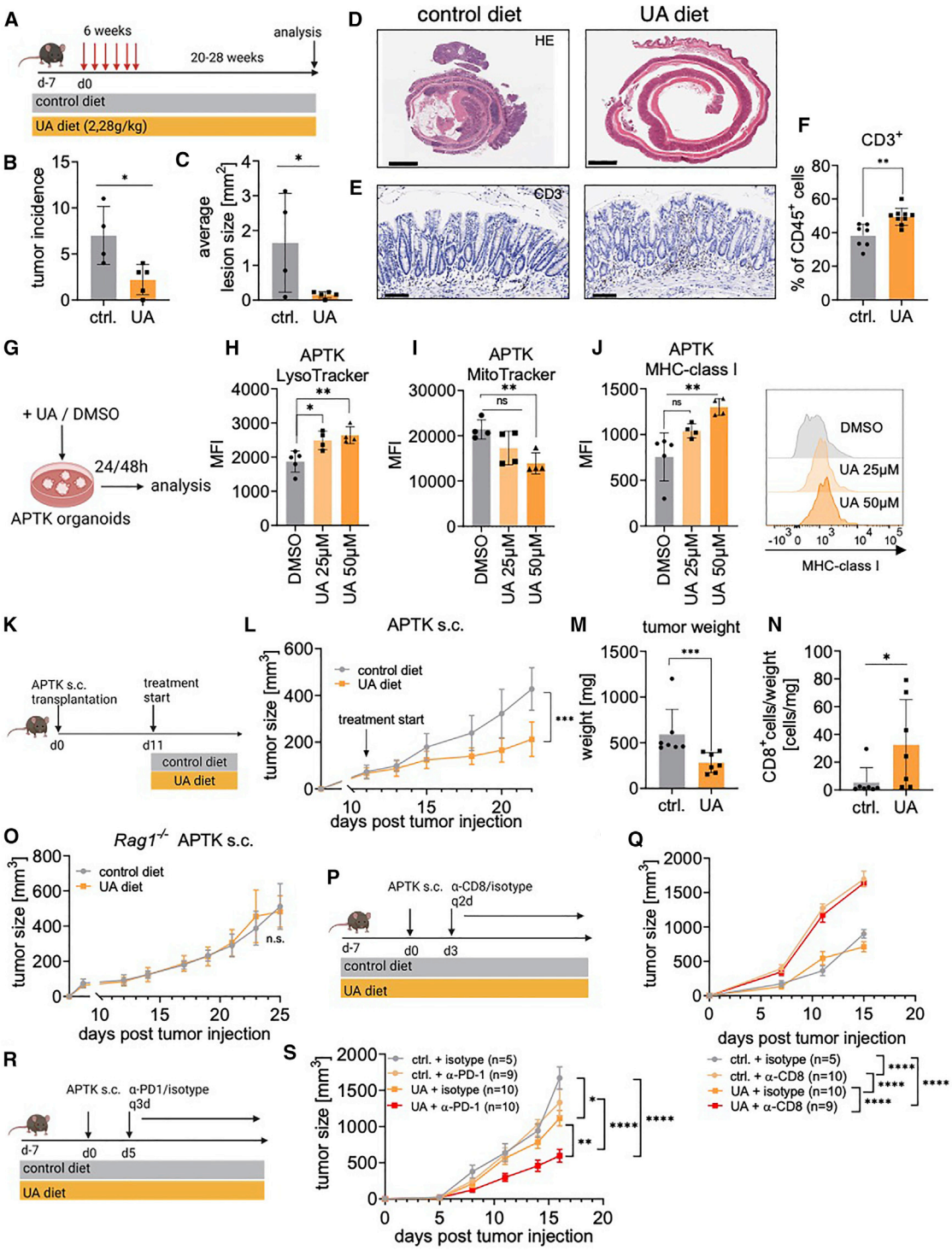

Figure 1. Oral UA confers anti-tumor effects in murine colorectal cancer in a T cell-dependent manner

(A) Schematic representation of AOM model and treatment regimen.

(B and C) Tumor incidence and average lesion size of AOM-induced tumors receiving a UA-containing diet or control diet. Data are mean ± SD, n = 4/5, *p < 0.05 by two-sided t test. One of two independent experiments shown.

(D) Representative images of swiss-roll sections from AOM-induced colon tumors. Scale bars, 2 mm.

(E) Representative images of $CD3^+$ T cell staining of colons from AOM-treated mice as depicted in (A) and (D). Scale bars, 100 μm.

(F) Relative number of $CD45^+CD3^+$ T cells in colons of AOM-treated mice at week 24. Data are mean ± SD, n = 7/8, **p < 0.01 by two-sided t test.

(G) Organoid treatment scheme. APTK organoids were incubated in the presence of UA or DMSO for the indicated time points, prior to flow cytometric analysis.

(legend continued on next page)

cells (DCs), tumor-associated macrophages (TAMs), or myeloid-derived suppressor cell (MDSC) subsets (Figures S2H–S2M). This indicates that UA directly acts on T cells, and their reduced exhaustion state is not simply a by-product of an altered TME in this model. Indeed, fitting the observation of self-dividing memory subsets (Kratchmarov et al., 2018; Utzschneider et al., 2016), we found increased expression of the transcription factor T cell factor 1, TCF1, in tumor-infiltrating $CD8^+$ T cells (Figure 2H), a hallmark of cytotoxic cells with retained stemness properties. Additionally, we observed a reduction of exhaustion markers such as PD-1, CTLA-4, and Tim3 in $CD8^+$ T cells of UA-fed mice (Figures 2I–2K), which allowed a stronger induction of TNF-α and IFNγ when tumor-infiltrating $CD8^+$ T cells were re-stimulated with PMA/ionomycin *ex vivo* (Figures 2L and 2M). Collectively, these data indicate that UA treatment results in the formation of T_{SCM} in the TME, conferring superior $CD8^+$-mediated anti-tumor immunity.

UA improves tumor therapy by adoptive T cell transfer

Adoptive cell transfer (ACT) represents the infusion of antigen-specific leukocytes with direct anti-tumor activity; however, identification, selection, and expansion of lymphocyte subsets harboring optimal anti-tumor qualities remains one of the most crucial challenges toward optimizing this therapeutic strategy (Rosenberg and Restifo, 2015). Adoptive cell transfer benefits especially from minimally differentiated cells due to their durability and long-term potential to generate unexhausted effector cells (Gattinoni et al., 2012; Mo et al., 2021; Roberto et al., 2015). In particular, $CD8^+$ T cells restricted in a stem-like state have been associated with enhanced tumor suppressive properties upon adoptive cell transfer (Gattinoni et al., 2011; Verma et al., 2021). Having demonstrated that UA induces a T_{SCM} phenotype in murine T cells, we next investigated whether UA could be exploited to improve adoptive immunotherapy. We cultured T cells from OT-1 donor mice (Figure 3A) for 48 h in the presence of UA or vehicle control, followed by adoptive transfer into immundeficient *Rag1*$^{-/-}$ mice. Prior to ACT, $CD8^+$ T cells from OT-1 donors also displayed a T_{SCM} phenotype (Figures S3A and S3B) with enhanced CD95 expression (Figure S3C). 7 days following the transfer, the number of engrafted $CD8^+$ T cells was higher in mice that had received UA-treated T cells (Figure 3B) supporting an increased potential to expand. Moreover, when UA-conditioned OT-1 T cells were transplanted into mice bearing palpable ovalbumin-overexpressing APTK (APTK-OVA) tumors (Figure 3C), this led to greater tumor suppression compared to control OT-I T cells (Figures 3D and 3E). Analysis of tumors revealed upon UA-T cell transfer a lower expression of CD44 and a higher number of $TCF1^{Hi}CD8^+$ tumor-infiltrating T cells (Figures 3F and 3G). This is in tumors in line with maintenance of a UA-induced memory phenotype (Schumann et al., 2015; Zhou et al., 2010). CD62L expression remained unchanged (Figure 3H). Moreover, consistent with an improved memory response, animals receiving UA-pretreated T cells contained less $Tim3^{Hi}PD1^{Hi}$ terminally exhausted $CD8^+$ T cells in the TME (Figure 3I). Thus, UA augments immune-mediated anti-tumor memory upon adoptive cell transfer.

Urolithin A induces Pink1-dependent mitophagy in T cells

Next, we examined whether the shift toward $CD44^-CD62L^+Sca1^{Hi}$ T_{SCM} cells was triggered by UA-induced mitophagy in T cells. We confirmed a reduction of mitochondrial membrane potential within six h after UA administration in $CD8^+$ T cells (Figures 4A and 4B). This was accompanied by enhanced lysosome formation (Figure 4C) and after 24 h followed by the loss of mitochondrial content in a dose-dependent manner (Figure 4D). The latter could be detected in all T cell subsets analyzed (T_{SCM}, T_{CM}, and T_{EFF}; Figure 4E), thus suggesting induction of mitophagy.

UA activates mitophagy in myocytes and hippocampal neurons via a Pink1/Parkin-mediated stress response (D'Amico et al., 2021). Similarly in αCD3/αCD28 stimulated T cells, UA led to a significant upregulation of *Atg5*, *Atg7*, *p62*, *Lamp2*, and *Pink1* gene expression (Figure 4F). Moreover, UA stabilized Parkin protein expression (Figure 4G). To functionally confirm the dependence

(H) Quantification of lysosome formation as assessed by LysoTracker MFI via flow cytometry after 24 h incubation at the presence of various UA concentrations. Data are mean ± SD, n = 5/4/4, *p < 0.05, **p < 0.01 by one-way ANOVA followed by Tukey's multiple comparison test. Representative results from one of two independent experiments are shown.

(I and J) (I) MitoTracker signal of APTK organoids incubated for 24 h in the presence of UA *in vitro* (n = 4/4/4) and antigen presentation via MHC-I molecules (J) after 48 h of treatment (n = 5/4/4). Data are mean ± SD, **p < 0.01 by one-way ANOVA followed by Tukey's multiple comparison test. Results from one of two independent experiments are shown.

(K) Experimental setup of oral UA administration in mice with established APTK-s.c. tumors. Treatment diet was initiated 11 days after tumor injection and maintained until the end of the experiment.

(L) Growth curve of mice subcutaneously transplanted with APTK tumors, receiving either UA-containing or control food. Data are mean ± SD, n = 7, ***p < 0.001 by two-sided t test. One of two independent experiments are shown.

(M and N) (M) End point tumor weight, (N) $CD8^+$ T cell infiltration in APTK-s.c. tumors assessed by flow cytometry, normalizing total number of $CD8^+$ T cells to tumor weight. Data are mean ± SD, n = 7, *p < 0.05 and ***p < 0.001 by Mann-Whitney test.

(O) Size of subcutaneous APTK tumors in *Rag1*$^{-/-}$ mice receiving UA-containing or control food. Treatment was initiated as depicted in (K). Data are mean ± SD, n = 7, depicting one of two independent experiments.

(P) $CD8^+$ T cell depleting or isotype control antibodies were applied every 2 days starting 3 days after s.c. injection of APTK organoids in C57BL/6 mice.

(Q) Effect of $CD8^+$ T cell depletion on size of subcutaneous APTK tumors in C57BL/6 mice receiving UA-containing or control food. Data are mean ± SEM, isotype n = 5, UA food + α-CD8 n = 9, other groups n = 10, ****p < 0.0001 by one-way ANOVA followed by Tukey's multiple comparison test. Data shown represents pooled data from two experiments with comparable results.

(R) α-PD-1 or isotype antibodies were injected every 3 days starting 5 days after s.c. injection of APTK organoids in C57BL/6 mice.

(S) Effect of α-PD-1 treatment on size of subcutaneous APTK tumors in C57BL/6 mice receiving UA-containing or control food. Data are mean ± SEM, isotype n = 5; control food + α-PD-1 n = 9; other groups n = 10; *p < 0.05, **p < 0.01, and ****p < 0.0001 by one-way ANOVA followed by Tukey's multiple comparison test. Data shown represents pooled data from two experiments with comparable results.

See also Figure S1.

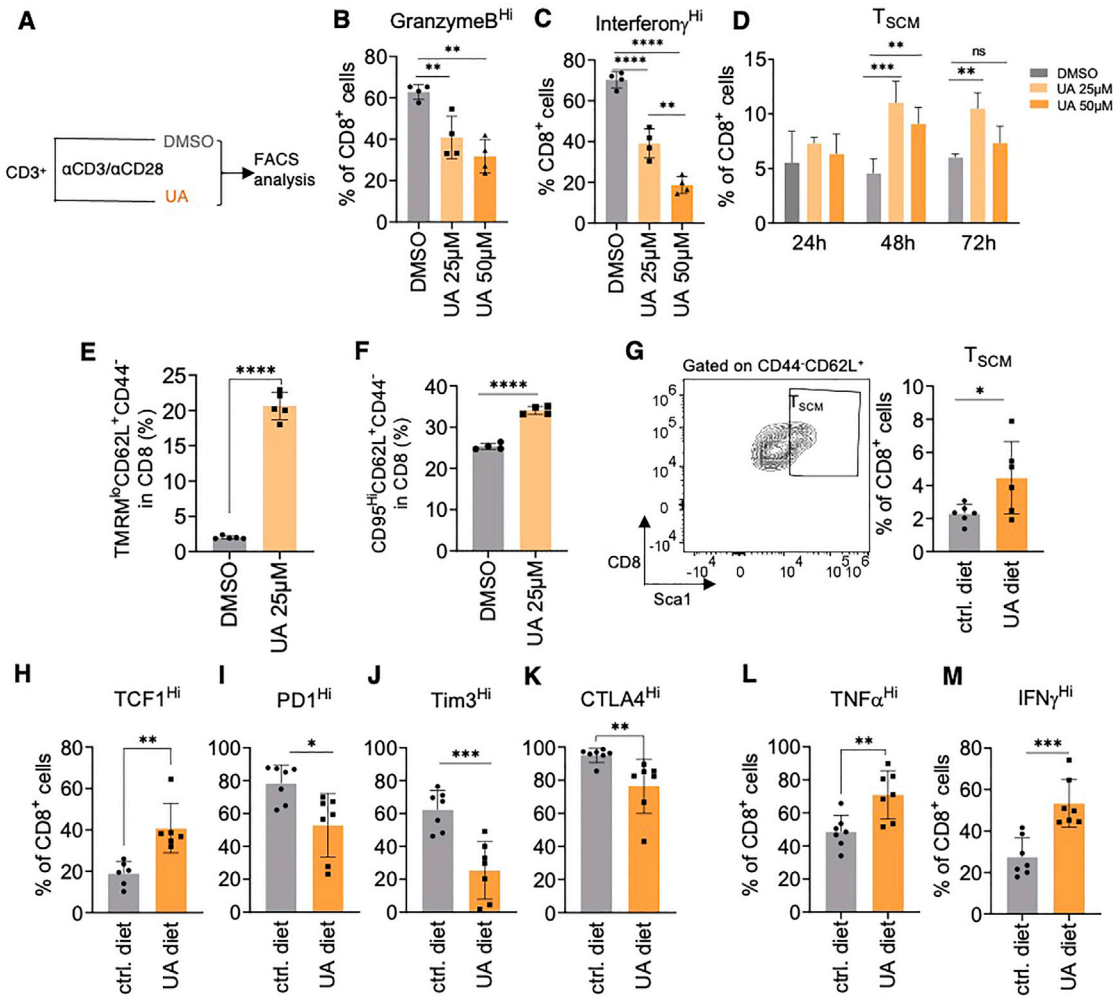

Figure 2. UA promotes T_{SCM} cell expansion

(A) Scheme of $CD3^+$ T cell activation, treatment, and analysis.

(B and C) Granzyme B and IFNγ expression in αCD3/αCD28 stimulated $CD3^+$ T cells in the presence of UA or DMSO after 48 h. Data are mean ± SD, n = 4, $^{**}p < 0.01$ and $^{****}p < 0.0001$ by one-way ANOVA followed by Tukey's multiple comparison test.

(D) Quantification of $CD44^-CD62L^+Sca1^{Hi}$ T_{SCM} 24, 48, and 72 h after αCD3/αCD28 stimulation. Data are mean ± SD, n = 4 from four independent experiments, $^{**}p < 0.01$; $^{***}p < 0.001$ by two-way ANOVA followed by Tukey's multiple comparison test.

(E) Frequency of $CD62L^+CD44^-CD8^+$ T cells with low mitochondrial membrane potential ($TMRM^{Lo}$) after 48 h in the presence or absence of UA (25 μM). Data are mean ± SD, n = 5; $^{****}p < 0.0001$ by two-sided t test.

(F) Frequency of $CD95^{Hi}CD62L^+CD44^-CD8^+$ T cells 48 h after in αCD3/αCD28 stimulation in the presence or absence of UA (25 μM). Data are mean ± SD; n = 5; $^{****}p < 0.0001$ by two-sided t test.

(G–K) (G) Frequency of T_{SCM} (n = 7), (H) TCF1 (n = 7), (I) $PD1^{Hi}$ (n = 6), (J) $Tim3^{Hi}$ (n = 6), and (K) $CTLA4^{Hi}$ (n = 6) within $CD8^+$ TIL of APTK-induced tumors receiving control or UA-containing diet. Data are mean ± SD, $^*p < 0.05$; $^{**}p < 0.01$; $^{***}p < 0.001$ by two-sided t test.

(L and M) (L) TNF-α and (M) IFNγ expression in $CD8^+$ TIL of APTK-induced tumors receiving control or UA-containing diet upon re-stimualtion with Phorbol 12-myristate 13-acetate (PMA)/ionomycin. Data are mean ± SD, n = 7 per group, $^{**}p < 0.01$ and $^{***}p < 0.001$ by two-sided t test.

See also Figure S2.

of UA-induced T_{SCM} formation on Pink1/Parkin-mediated mitophagy, we activated *Pink1*$^{-/-}$ T cells in the presence or absence of UA. Loss of *Pink1* prevented the UA-induced lysosome formation as well as the decrease in mitochondrial content (Figures 4H and 4I). *Pink1*$^{-/-}$ $CD8^+$ T cells failed to exhibit a T_{SCM} phenotype (Figure 4J) and expressed less TCF1 in $CD44^-CD62L^+CD8^+$ T cells (Figure 4K). Consequently, *Pink1* deletion abrogated the tumor suppressive effect of UA (Figure 4L), whereas $CD8^+$ TIL of *Pink1*$^{-/-}$ mice did not exhibit differences in TCF1 expression, exhaustion markers, or *ex vivo* cytokine release (Figures 4M–4Q). These data strongly support the notion that UA-induced Pink1-dependent mitophagy triggers T_{SCM} formation to enhance anti-tumor immunity.

UA induces T_{SCM} via cytosolic release of Pgam5 that drives Wnt signaling

To explore the downstream events linking mitophagy to T_{SCM} formation, we performed RNA sequencing (RNA-seq) to globally

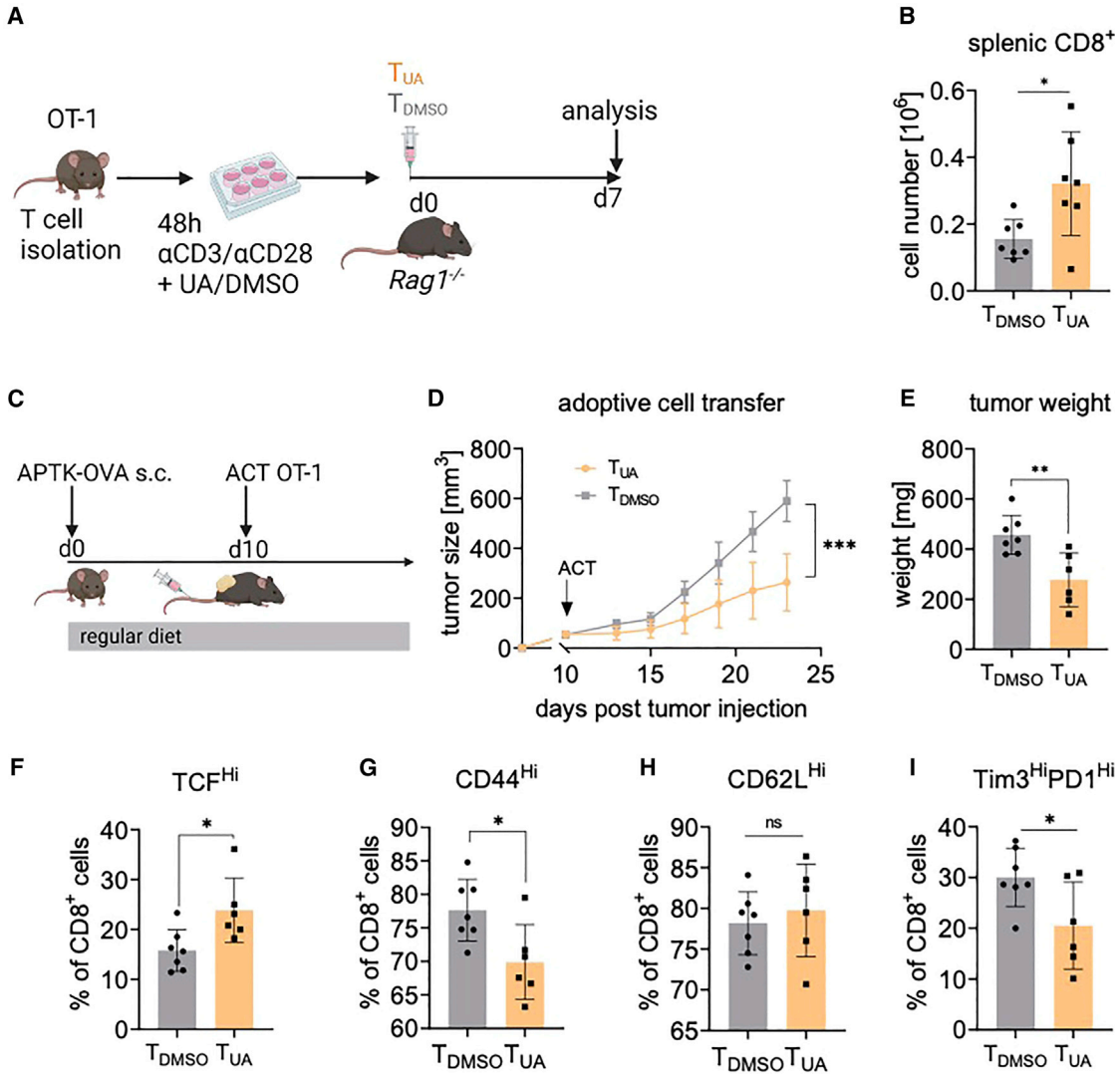

Figure 3. UA treatment augments efficacy of adoptive cell transfer (ACT)

(A) Experimental setup of adoptive cell transfer into *Rag1*$^{-/-}$ mice: CD3$^+$ T cells from OT-1 donor mice were stimulated for 48 h with αCD3/αCD28 in the presence of UA (25 μM; T_{UA}) or DMSO (T_{DMSO}) prior to transfer.

(B) Number of splenic CD8$^+$ T cells in *Rag1*$^{-/-}$ mice 1 week after adoptive transfer of either UA-treated or control T cells. Data are mean ± SD with n = 7 per group, *p < 0.05 by two-sided t test.

(C) Experimental setup of adoptive cell transfer of OT-1 CD3$^+$ T cells in mice bearing APTK-OVA s.c. tumors. *Ex vivo* stimulation prior to transfer was performed as depicted in (A).

(D) Growth curve of s.c. APTK-OVA tumors treated as depicted in (C), UA: n = 6, DMSO: n = 7, Data are mean ± SD, ***p < 0.001 by two-sided t test.

(E) Final tumor weight of s.c. transplanted APTK-OVA tumors in *Rag1*$^{-/-}$ mice transplanted with T_{UA} or T_{DMSO}. Data are mean ± SD, n = 6-7, **p < 0.01 by two-sided t test.

(F–H) Analysis of TIL of ACT-treated *Rag1*$^{-/-}$ mice carrying APTK-OVA tumors: (F) expression of CD44, (G) TCF1 and (H) CD62L in CD8$^+$ TIL from APTK-OVA induced tumors that had received UA-treated OT-I T cells (n = 6) or DMSO-treated OT-I T cells (n = 7), data are mean ± SD, *p < 0.05 by two-sided t test, n.s. not significant.

(I) Frequency of exhausted Tim3^{Hi}PD-1^{Hi} CD8$^+$ TIL from APTK-OVA induced tumors that had received UA-treated OT-I T cells (n = 6) or DMSO-treated OT-I T cells (n = 7). Data are mean ± SD, *p < 0.05 by two-sided t test.

See also Figure S3.

assess differential gene expression in T cells exposed for 48 h to either DMSO or UA *in vitro*. We identified a total number of 1,178 differentially expressed genes of which 765 were upregulated and 413 downregulated (Figure 5A). UA treatment reduced the expression of genes that code for immune checkpoints and effector molecules, whereas enhanced the expression of *Cd27*, *Ccr7*, and adhesion genes (Figure 5B), a characteristic of stem cell-like CD8$^+$ T cells (Gattinoni et al., 2011; Mo et al., 2021; Parisi et al., 2020; Reschke et al., 2021). Additionally, UA-treated cells revealed an enrichment of genes involved in memory formation such as *Tcf7*, *Bach2*, and *Bcl6* and reduced expression of effector fate associated genes *Prdm1* and *Id2*

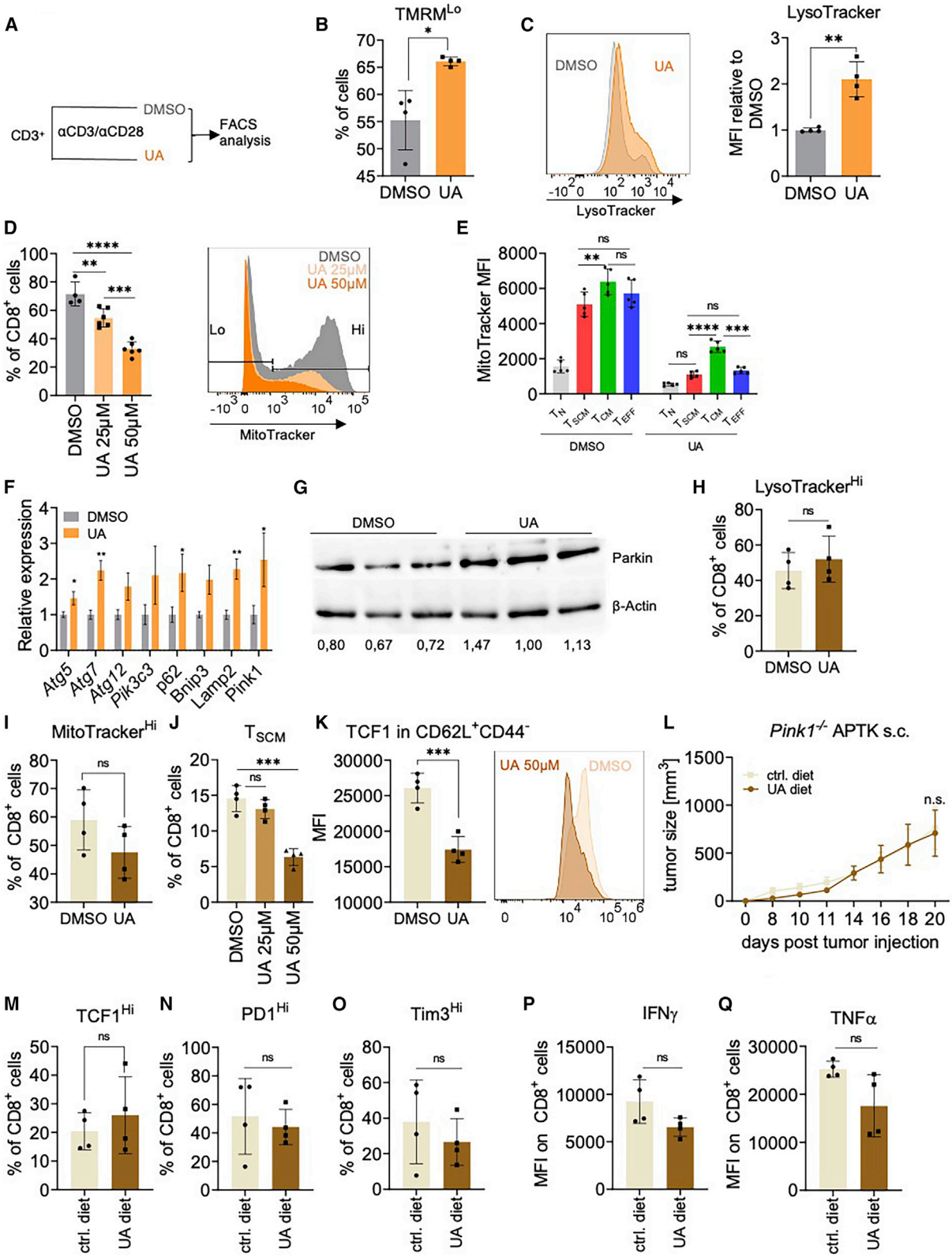

Figure 4. Urolithin A triggers Pink1-dependent mitophagy in T cells

(A) Scheme of CD3+ T cell activation, treatment, and analysis.

(B) Frequency of CD8+ T cells with low mitochondrial membrane potential (TMRMLo) after 6-h stimulation with αCD3/αCD28 in the absence or presence of UA (50 μM). Data are mean ± SD, n = 4; *p < 0.05 by two-sided t test. Data shown represent one of two independent experiments.

(legend continued on next page)

(Ichii et al., 2002; Roychoudhuri et al., 2016; Zhou et al., 2010; Figure 5C). In agreement with the increased number of TCF1^{Hi} T_{SCM} cells, upstream regulator analysis of RNA-seq data revealed *Tcf7* as a possible regulator of UA-induced transcriptomic changes on T cells *in vitro* (Figure S4A). Indeed, when we applied ICG001 to pharmacologically block TCF1, UA-induced T_{SCM} formation *in vitro* was abrogated (Figures 5D and 5E).

Next, we examined whether the observed upregulation of TCF1 was a result of enhanced Wnt signaling. In line with this notion, we observed an increased transcription of several Wnt target genes (extended data Figure 4B). Moreover, UA led to a marked decrease of β-catenin phosphorylation already after 6 h (Figure 5F), indicating the activation of Wnt signaling prior to the transcriptional changes. Mitophagy releases the mitochondrial-bound protein phosphatase *phosphoglycerate mutase family member 5* (Pgam5) to the cytoplasm where it has been suggested to block axin-dependent β-catenin degradation thereby inducing mitochondrial biogenesis (Bernkopf et al., 2018; Yamaguchi et al., 2019). To explore whether Pgam5 may be involved in UA-induced Wnt activation, we examined Pgam5 localization upon UA administration. Immunoblot analysis of sub-cellular fractionations revealed that Pgam5 was indeed rapidly released into the cytoplasma upon UA-mediated mitophagy (Figure 5G), which could also be confirmed by immunofluorescence (Figure 5H). More importantly, *Pgam5* loss blocked the UA-dependent expansion of CD44^{-}CD62L^{+}Sca1^{Hi} T_{SCM} cells (Figure 5I). UA-treated *Pgam5*$^{-/-}$ CD8^{+} T cells failed to upregulate TCF1 or the memory marker CD95 *in vitro* (Figures 5J and 5K; Figure S4C), despite the fact that UA still enhanced lysosome formation and reduced mitochondrial content (Figures S4D and S4E), confirming that cytosolic Pgam5 contributed to UA-induced alterations of T cell function. In line with this notion, we confirmed lack of cytoplasmic expression of Pgam5 in *Pink1*$^{-/-}$ CD8^{+} T cells upon UA exposure (Figure S4F).

Pgam5-dependent Wnt activation is suggested to trigger compensatory mitochondrial biogenesis in response to mitophagy (Bernkopf et al., 2018). Peroxisome proliferator-activated receptor gamma coactivator 1-alpha (PGC-1α) is considered the master regulator of mitochondrial biogenesis (Finck and Kelly, 2006). Accordingly, we detected a marked upregulation of PGC-1 after prolonged UA administration *in vitro* (Figure 5L). This was accompanied by an increased mitochondrial content in TIL of APTK tumors (Figure 5M), indicating mitochondrial biogenesis and in line with superior T cell fitness in the TME (Dumauthioz et al., 2021; Scharping et al., 2016). UA failed to enhance PGC-1α in *Pink1*$^{-/-}$ or *Pgam5*$^{-/-}$ CD8^{+} T cells (Figures 5N and 5O; Figures S4G and S4H), whereas chemical inhibition of PGC-1α blocked UA-dependent expansion of CD44^{-}CD62L^{+}Sca1^{Hi} T_{SCM} cells (Figure 5P). Collectively, these results indicated that UA drives T_{SCM} formation via a Wnt-dependent upregulation of PGC-1α, promoted by the cystosolic release of Pgam5 in response to mitophagy.

UA promotes human T_{SCM} cells, facilitating generation of potent CAR T_{SCM}

Finally, we aimed to determine whether UA causes expansion of T_{SCM} cells in human CD8^{+} T cells. We isolated human CD3^{+} T cells from peripheral blood mononuclear cells (PBMCs) of healthy donors and stimulated them with αCD3/αCD28 beads *in vitro* in the presence of UA (Figure 6A). Indeed, UA increased the frequency of human T_{SCM} cells based on the expression of CD45RA^{+}CCR7^{Hi}CD62L^{+}CD95^{+}CD8^{+} in five of five individual donors (Figure 6B; Figures S5A and S5B). As in murine T cells, after 48 h of UA treatment, human CD8^{+} T cells displayed a decreased mitochondrial membrane potential (Figure 6C) and intracellular staining confirmed increased TCF1 expression (Figure 6D), validating that UA induces memory stem cell features in both murine and human T cells.

Infusion of T cells carrying an engineered chimeric antigen receptor (CAR), designed to specifically guide leukocytes to recognize and eliminate malignancies of interest, has shown impressive clinical results, but incomplete remissions and frequent relapses after successful therapy highlight the need to

(C) Quantification of lysosome formation in CD8^{+} T cells after 6 h stimulation with αCD3/αCD28 in the absence or presence of UA (50 μM). Data are mean ± SD, n = 4; **p < 0.01 by two-sided t test. Data shown represent one of two independent experiments.
(D) Frequency of MitoTracker Red staining of CD8^{+} T cells after 24 h stimulation with αCD3/αCD28 in the absence or presence of UA. Data are mean ± SD, n = 6 (UA) or n = 4 (DMSO), **p < 0.01, ***p < 0.001, ****p < 0.0001 by one-way ANOVA followed by Tukey's multiple comparison test.
(E) MitoTracker expression in T cell subsets 24 h after stimulation with αCD3/αCD28 in the absence or presence of UA. Data are mean ± SD, n = 5, **p < 0.01, ***p < 0.001, ****p < 0.0001 by one-way ANOVA followed by Tukey's multiple comparison test.
(F) qPCR analysis of various autophagy/mitophagy associated genes in T cells 24 h after stimulation with αCD3/αCD28 in the absence or presence of UA (50 μM). Data are ± SEM, n = 3; *p < 0.05,**p < 0.01 by two-sided t test.
(G) Immunoblot analysis of indicated proteins in T cells 24 h after stimulation with αCD3/αCD28 in the absence or presence of UA (50 μM).
(H) Quantification of lysosome formation in *Pink1*$^{-/-}$ CD8^{+} T cells after 6 h stimulation with αCD3/αCD28 in the absence or presence of UA (50 μM). Data are mean ± SD, n = 4, n.s., not significant by two-sided t test. Data shown represent one of two independent experiments.
(I) Frequency of MitoTracker^{Hi} *Pink1*$^{-/-}$ CD8^{+} T cells after 48 h stimulation with αCD3/αCD28 in the absence or presence of UA (50 μM). Data are mean ± SD, n = 4, n.s. not significant by two-sided t test. Data shown represent one of two independent experiments.
(J) Frequency of T_{SCM} in *Pink1*$^{-/-}$ CD8^{+} T cells after 48 h stimulation with αCD3/αCD28 in the absence or presence of UA (25 and 50 μM). Data are mean ± SD, n = 4, ***p < 0.001 by two-sided t test.
(K) Expression of TCF1 in CD62L^{+}CD44^{-}CD8^{+} cells from *Pink1*$^{-/-}$ mice after 48 h stimulation with αCD3/αCD28 in the absence or presence of UA (50 μM). Data are mean ± SD, n = 4, ***p < 0.001 by two-sided t test.
(L) Growth curve of *Pink1*$^{-/-}$ mice s.c. injected with APTK organoids, fed UA-containing or control diet as depicted in Figure1K. Data are mean ± SD, n = 4/group; n.s. not significant by two-sided t test.
(M–O) (M) Frequency of TCF^{Hi}, (N) PD^{Hi}, (O) Tim3^{Hi} CD8^{+} TIL in APTK-induced tumors in *Pink1*$^{-/-}$ mice fed either UA or control diet. Data are mean ± SD, n = 4/group.
(P and Q) (P) Expression of IFNγ and (Q) TNF-α *in* CD8^{+} TIL from *Pink1*$^{-/-}$ restimulated *ex vivo* with PMA/ionomycin in the presence of brefeldin A for 3 h. Data are mean ± SD, n = 4.

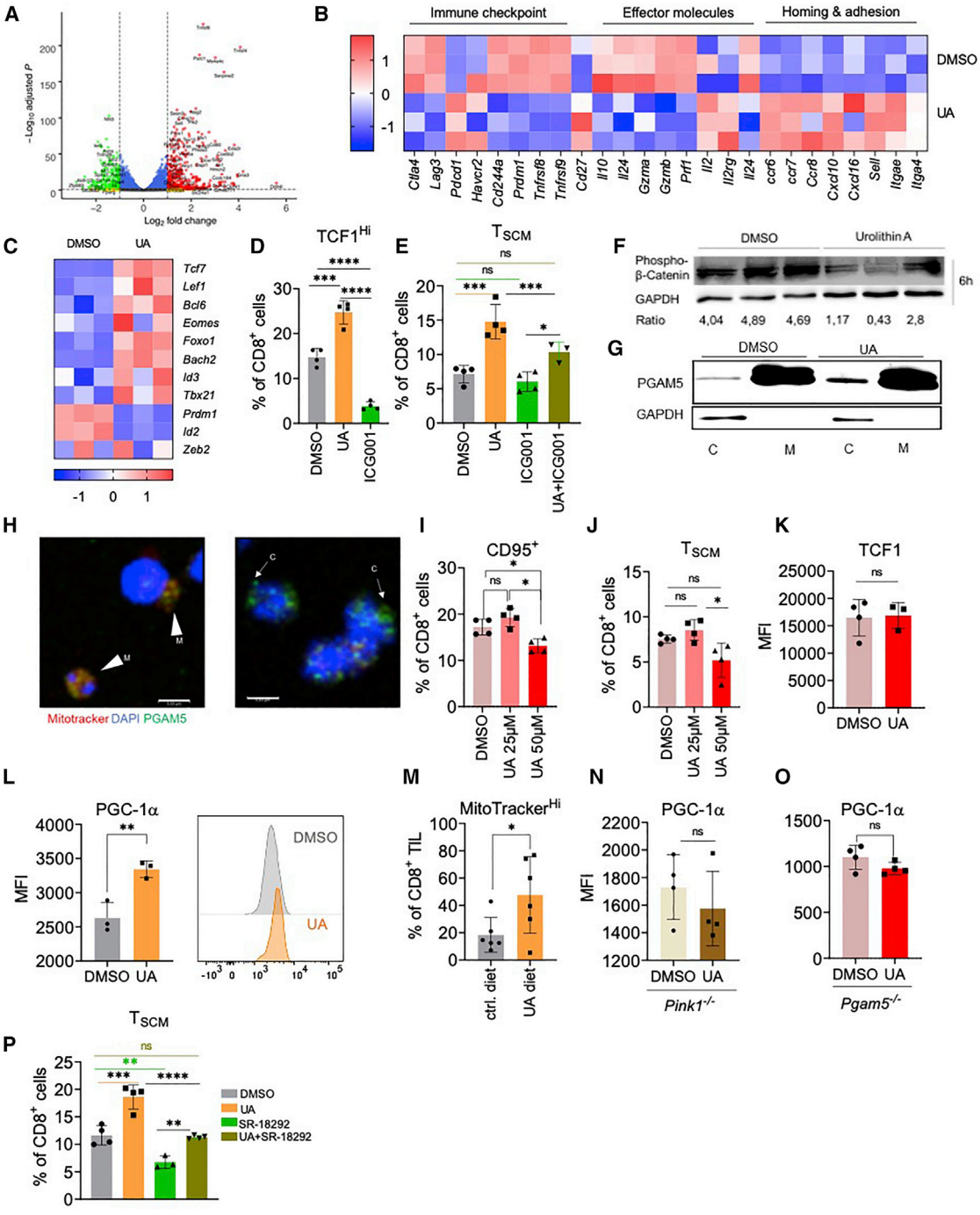

Figure 5. UA-induced T_{SCM} expansion is due to cytosolic release of PGAM5 that drives Wnt signaling

(A) Enhanced volcano plot of RNA-seq of T cells stimulated for 48 h with αCD3/αCD28 in the absence or presence of UA (50 μM). A $\log_2$-fold change of 1, and a p value of $p < 0.05$ were considered significant (red, significantly upregulated in UA-treated cells; green, significantly upregulated in DMSO-treated cells); n = 3 per group.

(B) Heatmap of differentially expressed genes associated with immune checkpoints, effector molecules, and genes coding for leukocyte migration.

(C) Heatmap of differentially expressed genes associated with T cell memory versus effector fate decisions. Data underwent *Z* score normalization for display (n = 3 per group).

(D) Frequency of $TCF1^{Hi}$ expressing $CD8^+$ T cells after 48 h stimulation with αCD3/αCD28 in the presence of UA (50 μM) or the TCF1 inhibitor ICG001 (10 μM) in comparison to DMSO control. Data are mean ± SD, n = 4, ***p < 0.001; ****p < 0.0001 by one-way ANOVA followed by Tukey's multiple comparison test.

(E) Frequency of T_{SCM} after 48 h stimulation with αCD3/αCD28 in the presence of UA (50 μM) and the TCF1 inhibitor ICG001 (10 μM) in comparison to DMSO control. Data are mean ± SD, n = 4: DMSO, UA, ICG001, n = 3: UA+ICG001, *p < 0.05, ***p < 0.001; n.s. not significant by one-way ANOVA followed by Tukey's multiple comparison test. One of two independent experiments are shown.

(legend continued on next page)

improve sustained anti-tumor response (June et al., 2018; Majzner and Mackall, 2019). CAR T cells containing high fractions of $T_{N/SCM}$ are suggested to show improved tumor killing and the exclusive ability to counteract leukemia re-challenge in hematopoietic stem/precursor cell-humanized mice (Arcangeli et al., 2022). To determine whether UA-triggered mitophagy also constitutes a feasible strategy to induce CAR-T_{SCM}, activated T cells were transduced with the CD19-CAR gene by a lentiviral vector (VSV-LV) in the presence or absence of UA. 3 days post transduction, the amount of CAR-expressing T_{SCM} was determined (Figure 6E; Figure S5C). UA did not impair gene delivery into $CD8^+$ cells (Figure S5D); however, although CAR-expressing T_{SCM} cells were markedly increased and comprised about 60% of $CD8^+$ cells upon UA exposure (Figure 6F), this did not have a negative impact on CD19 CAR T cell-mediated killing of NALM-6 leukemia cells (Figure 6G). Markers of exhaustion were not affected by UA supplementation (Figures S5C and S5E). Even when we applied UA to previously frozen CAR T cells specific for carcinoembryonic antigen (CEA; Figure 6H), this strongly enhanced CAR T_{SCM} formation (Figure 6I) with comparable killing efficacy of CEA-expressing human CRC organoids (Figure 6J). Thus, UA markedly enhances expansion of CAR-T_{SCM} cells.

DISCUSSION

UA is suggested as an encouraging nutrient addition to target age-related conditions (D'Amico et al., 2021). In various preclinical models, UA has been proven effective in attenuating inflammation and improving muscle, brain, and joint functions. In addition to this wide spectrum of potential applications covering the fields of neuro-degeneration, muscle disorders, and inflammatory diseases, we demonstrate here that UA induces a protective anti-tumor $CD8^+$ T cell immunity strongly supporting its benefit for cancer therapy either in combination with immune checkpoint blockade or in the context of adoptive T cell therapy. Moreover, we suggested mitophagy in IEC as an important mechanism to enhance antigen presentation during early intestinal tumorigenesis. Our data here expanded upon this work and suggested that mitophagy induction represents an attractive option for therapy of established tumors as it promotes an adaptive T cell response via a dual mechanism: enhancing antigen presentation in tumor epithelia as well as directly affecting T cell fate.

T_{SCM} cells are thought to enhance immunity by constantly giving rise to less exhausted effector T cells in the TME (Gattinoni et al., 2017). Multiple pathways are expected to govern T cell fate decisions, balancing between stemness and terminal differentiation (Gattinoni et al., 2012; Pilipow et al., 2018; Scholz et al., 2016). We propose a complex interplay linking intrinsic mitochondrial cues and subsequent activation of the stemness promoting Wnt-driven *Tcf7* transcription. The effect of UA on T_{SCM} formation appears to be both dependent on Pink1 and Pgam5. Interestingly, Pgam5 is suggested to regulate Pink1/Parkin-mediated mitophagy (Yu et al., 2020a); however, we observed adequate induction of mitophagy in *Pgam5*$^{-/-}$ $CD8^+$ T cells. Of note, we also observed that compensatory mitochondrial biogenesis second to mitophagy drives T cell stemness decisions. Wnt-β-Catenin signaling is suggested to induce mitochondrial biogenesis (Bernkopf et al., 2018). We propose PGC-1α as one critical regulator that is directly activated by Wnt signaling and essential to T_{SCM} formation as it has recently been proposed in the context of Mek inhibition (Verma et al., 2021). Similarly, we also observed a downregulation of cyclin D1 leading to an arrest of proliferation and effector differentiation (Gattinoni et al., 2009; Pilipow et al., 2018; Verma et al., 2021).

The concept of pharmacologically altering mitochondrial dynamics has been proven to be effective in the context of regulating cellular fate and function. Increased mitochondrial clearance via nicotinamide riboside (NR) could reinforce stem cell fate decisions in hematopoetic stem cells (HSCs) (Vannini et al., 2019) and improved responsiveness to anti-PD1 treatment (Yu et al., 2020b). Our data highlight the requirement of mitophagy for T_{SCM} formation and describe the downstream signaling pathway linking mitochondrial dynamics and adaptive immunity. Furthermore, we identified a novel potential application of UA due to its capacity to expand CAR T_{SCM} cells. CAR T_{SCM} cells confer an improved and sustained anti-tumor efficacy upon repeated exposure to tumor cells *in vivo* (Arcangeli et al., 2022). Furthermore, CAR-T_{SCM} cells are intrinsically less prone to induce severe cytokine release syndrome (Arcangeli et al., 2022). Such subsets are currently selected via cell sorting, thus constituting a costly and time-consuming manufacturing step (Abou-El-Enein et al., 2021). By the addition of UA after CAR gene transduction, we suggest a readily applicable, scalable method of rapidly generating potent CAR-T_{SCM} that avoids premature activation and exhaustion,

(F) Immunoblot analysis of phospho-β-catenin in T cells stimulated for 6 h with αCD3/αCD28 in the absence or presence of UA (50 μM).
(G) Immunoblot analysis of fractionated T cells stimulated for 6 h with αCD3/αCD28 in the absence or presence of UA (50 μM); c = cytosolic, m = mitochondrial fraction. Experiment was repeated twice.
(H) Immunofluorescence of PGAM5 (green) in T cells stimulated for 6 h with αCD3/αCD28 in the absence or presence of UA (50 μM). Cells were stained with MitoTracker Red to visualize mitochondria (m, mitochondrial localization; c, cytoplasmatic localization). Scale bars, 5 μm.
(I–K) Frequency of (I) T_{SCM}, (J) $CD95^+$, and (K) TCF1 expressing *Pgam5*$^{-/-}$ $CD8^+$ T cells after 48 h stimulation with αCD3/αCD28 in the absence or presence of UA. Data are mean ± SD, n = 4/group, *p < 0.05, n.s. not significant by one-way ANOVA followed by Tukey's multiple comparison test.
(L) PGC-1α expression in $CD8^+$ T cells after 48 h stimulation with αCD3/αCD28 in the absence or presence of UA (50 μM). Data are mean ± SD, n = 3, **p < 0.01 by two-sided t test. One of two independent experiments are shown.
(M) Mitochondrial content of $CD8^+$ TIL from APTK-induced tumors from *wt* mice fed UA or control diet as depicted in Figure 1K. Data are mean ± SD, n = 6/group, *p < 0.05 by two-sided t test.
(N and O) PGC-1α expression in $CD8^+$ T cells derived from *Pink1*$^{-/-}$ KO mice (N) or *Pgam5*$^{-/-}$ mice (O) after 48 h stimulation with αCD3/αCD28 in the absence or presence of UA (50 μM). Data are mean ± SD, n = 4.
(P) Frequency of T_{SCM} after 48 h stimulation with αCD3/αCD28 in the presence of UA (50 μM) or the PGC-1α inhibitor (PGC-1αi, 10 μM). Data are mean ± SD, n = 4, **p < 0.01, ***p < 0.001, ****p < 0.0001 n.s., not significant by one-way ANOVA followed by Tukey's multiple comparison test.
See also Figure S4.

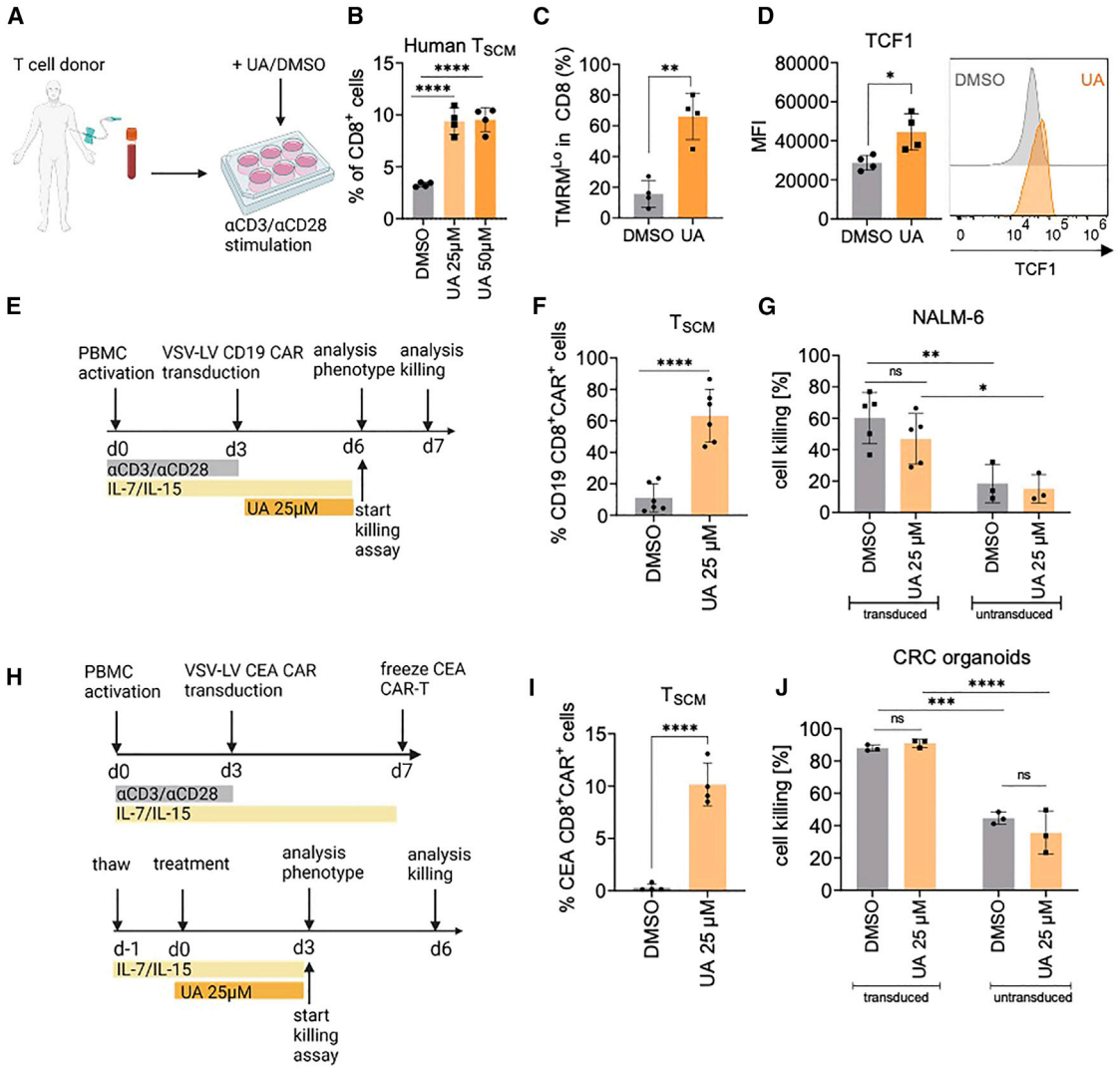

Figure 6. UA promotes human T_{SCM}, facilitating generation of potent CAR T_{SCM}

(A) Human PBMC were isolated from healthy donors, T cells were purified and stimulated *ex vivo* with αCD3/αCD28 in the presence of UA (50 μM) or DMSO control.

(B) Frequency of human T_{SCM} 48 h after stimulation as shown in (A). Data are mean ± SD, n = 4, ****p < 0.0001 by one-way ANOVA followed by Tukey's multiple comparison test.

(C) Quantification of human $TMRM^{lo}CD8^+$ T cells 48 h after stimulation in the presence of UA or DMSO control. Data are mean ± SD, n = 4,**p < 0.01 by two-sided t test.

(D) TCF1 expression in human $CD8^+$ T cells 48 h after stimulation in the presence of UA or DMSO control. Data are mean ± SD, n = 4,*p < 0.05 by two-sided t test. In (B), representative data of one out of five donors with comparable outcome are shown.

(E) Experimental layout of CD19-CAR T cell generation and expansion. PBMCS from healthy donors were expanded in the presence of IL-7/IL-15 for 3 days, followed by VSV-LV transduction. After 3 days of incubation, killing of Nalm-6 cells is assessed upon 24 h co-culture.

(F) Frequency of T_{SCM} within $CD19^-CAR^+CD8^+$ cells after generation as depicted in (E). Data are mean ± SD, n=6, ****p < 0.0001 by two-sided t test. Data are pooled from three independent experiments.

(G) Killing potential of CD19-CAR T cells. Percentage of dead NALM-6 cells upon 24 h co-culture with untransduced or CAR-transduced T cells ±UA/DMSO is shown. Data are mean ± SD, n = 5/3 (transduced/untransduced); *p < 0.05, **p < 0.01, ****p < 0.0001 by two-way ANOVA followed Sidak's multiple comparison test.

(H) Experimental layout of CEA-CAR T cell experiments. Following CAR gene transduction (upper panel), CAR T cells were frozen for subsequent experiments after thawing (lower panel).

(I) Frequency of T_{SCM} within CAR^+CD8^+ cells specific for CEA. Data are mean ± SD, n = 4, ****p < 0.0001 by two-sided t test. Data were pooled from two independent experiments.

(J) Killing potential of CEA-specific CAR T cells. Percentage of dead CEA-expressing human CRC organoids upon 72 h co-culture with untransduced or CAR-transduced T cells ±UA/DMSO is shown. Data are mean ± SD, n = 3; ***p < 0.001, ****p < 0.0001, n.s., not significant by two-way ANOVA followed Sidak's multiple comparison test.

See also Figure S5.

bypassing manufacturing challenges currently presenting an unmet need in CAR T cell therapy.

Previous studies have suggested *in vitro* antiproliferative and apoptotic activity of both pomegranate juice and purified elagitannins in CRC cell lines (Jaganathan et al., 2014; Seeram et al., 2005). Considering the particular limitations of ellagitannin metabolization into the bioavailable derivate UA, which shows large inter-individual variations due to the requirement of an adequate gut microbiome (Cortés-Martín et al., 2018), clinical applications of pomegranate juice and ellagitannins may be limited. Of note, concentrated forms of UA are associated with tumor-limiting properties both in pancreatic cancer cells *in vitro* and in murine PDAC upon oral gavaging, attributed to the suppression of the PI3K/AKT/mTOR pathway and alterations in the TME (Totiger et al., 2019). We demonstrate here that the effect of UA appears to be primarily dependent on $CD8^+$ T cells. This could be in part explained by a context specific sensitivity to mTOR inhibition as our colorectal tumor organoids are only partially responsive to mTOR inhibition (F.R.G., unpublished data). Nevertheless, the clear shift toward T_{SCM} cells suggests that UA-dependent anti-tumor immunity may not be limited to CRC. However, the complex inflammatory TME of the colon is characterized by a diverse interplay between tumor, immune, and stromal cells, as well as microbiome that governs carcinogenesis (Schmitt and Greten, 2021). Considering the broad effects of UA and its systemic nature (D'Amico et al., 2021), and *in vitro* evidence of UA affecting macrophage polarization (Boakye et al., 2018), we cannot exclude that other components that constitute the TME apart from $CD8^+$ T cells and antigen-expressing tumor cells may also be affected by UA in a biologically relevant manner.

Collectively, our study suggests that the orally available and well-tolerated mitophagy inducer UA confers $CD8^+$ T cell-dependent anti-tumor effects in CRC. The fact that UA induces a T_{SCM}-associated phenotype in human leukocytes and CAR T cells *ex vivo* indicates that our findings can be translated into human disease and provide a solid rationale for future clinical trials to examine whether oral UA supplementation or *in vitro* treatment of leukocytes can be used for more effective tumor therapy.

Limitations of the study

Although our study clearly demonstrates the link between mitophagy and T_{SCM} expansion, the exact mitochondrial target causing mitophagy remains to be identified as well as the proof that T_{SCM} expansion can be observed as a general consequence to other mitophagy inducing compounds regardless of their mode of action. Furthermore, we cannot exclude that UA impacts other non-mitochondrial targets that could potentially contribute to the observed phenotype. In the context of CAR T cell generation, UA proved to be a potent inducer of CAR-expressing T_{SCM}. Although others have demonstrated that the increased number of CAR-T_{SCM} should confer an improved anti-tumorigenic function when repeatedly challenged *in vivo* (Arcangeli et al., 2022), this awaits confirmation for *ex vivo* UA-treated CAR T cells in models of CRC and/or leukemia. In the future, it will be equally necessary to examine whether patients receiving such UA-treated CAR T cells will require additional oral UA administration.

STAR★METHODS

Detailed methods are provided in the online version of this paper and include the following:

- KEY RESOURCES TABLE
- RESOURCE AVAILABILITY
  - Lead contact
  - Materials availability
  - Data and code availability
- EXPERIMENTAL MODEL AND SUBJECT DETAILS
  - Mice
  - Human samples
- METHOD DETAILS
  - In vitro T cell isolation and stimulation
  - Organoids
  - Cell culture
  - Colorectal cancer models
  - Adoptive cell transfer
  - Lentiviral (LV) production
  - CAR gene delivery
  - CAR T cell killing assay
  - Tumor collection and sample preparation
  - Flow cytometry data acquisition
  - Quantitative PCR with reverse transcription analysis
  - RNA seq
  - Imaging
  - Histology
  - Protein analysis
- QUANTIFICATION AND STATISTICAL ANALYSIS

SUPPLEMENTAL INFORMATION

Supplemental information can be found online at https://doi.org/10.1016/j.immuni.2022.09.014.

ACKNOWLEDGMENTS

We thank Petra Dinse, Eva Rudolf, and Christin Danneil for expert technical assistance as well as the staff at the Animal Facility and the Histology Core Facilities at the Georg-Speyer-Haus for support and Anette Trzmiel for help with flow cytometry. We are thankful for NGS-Integrative Genomics Core Unit at the University Hospital Göttingen (Orr Shomroni) for performing total RNA-seq. P.K.Z. is supported by the Else-Kröner-Fresenius Foundation. C.B. was supported by DFG grant BE3686/9-1. Work in the lab of F.R.G. is supported by institutional funds from the Georg-Speyer-Haus, by the LOEWE Center Frankfurt Cancer Institute (FCI) funded by the Hessen State Ministry for Higher Education, Research, and the Arts (III L 5 - 519/03/03.001 - (0015)), Deutsche Forschungsgemeinschaft (FOR2438: Gr1916/11-1; SFB 1177, SFB1292-Project ID: 318346496-TP16; SFB1479-Project ID: 441891347-P02; GRK2336) and the ERC (Advanced Grant PLASTICAN-101021078). The Institute for Tumor Biology and Experimental Therapy, Georg-Speyer-Haus is funded jointly by the German Federal Ministry of Health and the Ministry of Higher Education, Research and the Arts of the State of Hessen (HMWK).

AUTHOR CONTRIBUTIONS

Conceptualization, D.D., V.P., and F.R.G.; methodology, D.D., V.P., A.M.N., P.K.Z., and F.R.G.; investigation, D.D., V.P., A.B., A.K., K.M., A.M.N., P.K.Z., M.D., and C.C.; resources, C.J.B., H.F.F., C.B., M.F.N., P.A.A., and C.R.; writing – original draft, D.D., V.P., and F.R.G.; visualization, D.D. and F.R.G.; supervision and funding acquisition, F.R.G.

DECLARATION OF INTERESTS

The authors have filed patents regarding the use of Urolithin in tumor therapy and CAR T cell generation. M.D. is an employee of AstraZeneca, UK. C.R. is CEO and a board member of Amazentis SA; P.A.A. is an employee of Vandria SA. F.R.G. has received consulting fees from Amazentis.

INCLUSION AND DIVERSITY

We support inclusive, diverse, and equitable conduct of research.

Received: March 1, 2022
Revised: July 31, 2022
Accepted: September 23, 2022
Published: October 18, 2022

REFERENCES

Abou-El-Enein, M., Elsallab, M., Feldman, S.A., Fesnak, A.D., Heslop, H.E., Marks, P., Till, B.G., Bauer, G., and Savoldo, B. (2021). Scalable manufacturing of CAR T cells for cancer immunotherapy. Blood Cancer Discov. *2*, 408–422. https://doi.org/10.1158/2643-3230.BCD-21-0084.

Andreux, P.A., Blanco-Bose, W., Ryu, D., Burdet, F., Ibberson, M., Aebischer, P., Auwerx, J., Singh, A., and Rinsch, C. (2019). The mitophagy activator urolithin A is safe and induces a molecular signature of improved mitochondrial and cellular health in humans. Nat. Metab. *1*, 595–603. https://doi.org/10.1038/s42255-019-0073-4.

Arcangeli, S., Bove, C., Mezzanotte, C., Camisa, B., Falcone, L., Manfredi, F., Bezzecchi, E., El Khoury, R., Norata, R., Sanvito, F., et al. (2022). CAR T-cell manufacturing from naive/stem memory T-lymphocytes enhances antitumor responses while curtailing cytokine release syndrome. J. Clin. Invest. *132*, e150807. https://doi.org/10.1172/JCI150807.

Bernkopf, D.B., Jalal, K., Brückner, M., Knaup, K.X., Gentzel, M., Schambony, A., and Behrens, J. (2018). Pgam5 released from damaged mitochondria induces mitochondrial biogenesis via Wnt signaling. J. Cell Biol. *217*, 1383–1394. https://doi.org/10.1083/jcb.201708191.

Boakye, Y.D., Groyer, L., and Heiss, E.H. (2018). An increased autophagic flux contributes to the anti-inflammatory potential of urolithin A in macrophages. Biochim. Biophys. Acta Gen. Subj. *1862*, 61–70. https://doi.org/10.1016/j.bbagen.2017.10.006.

Buck, M.D., O'Sullivan, D., Klein Geltink, R.I., Curtis, J.D., Chang, C.H., Sanin, D.E., Qiu, J., Kretz, O., Braas, D., van der Windt, G.J.W., et al. (2016). Mitochondrial dynamics controls T cell fate through metabolic programming. Cell *166*, 63–76. https://doi.org/10.1016/j.cell.2016.05.035.

Chen, D.S., and Mellman, I. (2017). Elements of cancer immunity and the cancer-immune set point. Nature *541*, 321–330. https://doi.org/10.1038/nature21349.

Cortés-Martín, A., García-Villalba, R., González-Sarrías, A., Romo-Vaquero, M., Loria-Kohen, V., Ramírez-de-Molina, A., Tomás-Barberán, F.A., Selma, M.V., and Espín, J.C. (2018). The gut microbiota urolithin metabotypes revisited: the human metabolism of ellagic acid is mainly determined by aging. Food Funct. *9*, 4100–4106. https://doi.org/10.1039/C8FO00956B.

D'Amico, D., Andreux, P.A., Valdés, P., Singh, A., Rinsch, C., and Auwerx, J. (2021). Impact of the natural compound urolithin A on health, disease, and aging. Trends Mol. Med. *27*, 687–699. https://doi.org/10.1016/j.molmed.2021.04.009.

Dumauthioz, N., Tschumi, B., Wenes, M., Marti, B., Wang, H., Franco, F., Li, W., Lopez-Mejia, I.C., Fajas, L., Ho, P.-C., et al. (2021). Enforced PGC-1α expression promotes CD8 T cell fitness, memory formation and antitumor immunity. Cell. Mol. Immunol. *18*, 1761–1771. https://doi.org/10.1038/s41423-020-0365-3.

Espín, J.C., Larrosa, M., García-Conesa, M.T., and Tomás-Barberán, F. (2013). Biological significance of urolithins, the gut microbial ellagic Acid-derived metabolites: the evidence so far. Evid. Based Complement. Alternat. Med. *2013*, 270418. https://doi.org/10.1155/2013/270418.

Finck, B.N., and Kelly, D.P. (2006). PGC-1 coactivators: inducible regulators of energy metabolism in health and disease. J. Clin. Invest. *116*, 615–622. https://doi.org/10.1172/JCI27794.

Gamero, A.M., and Larner, A.C. (2000). Signaling via the T cell antigen receptor induces phosphorylation of Stat1 on serine 727. J. Biol. Chem. *275*, 16574–16578. https://doi.org/10.1074/jbc.M910149199.

Gattinoni, L., Klebanoff, C.A., and Restifo, N.P. (2012). Paths to stemness: building the ultimate antitumour T cell. Nat. Rev. Cancer *12*, 671–684. https://doi.org/10.1038/nrc3322.

Gattinoni, L., Lugli, E., Ji, Y., Pos, Z., Paulos, C.M., Quigley, M.F., Almeida, J.R., Gostick, E., Yu, Z., Carpenito, C., et al. (2011). A human memory T cell subset with stem cell-like properties. Nat. Med. *17*, 1290–1297.

Gattinoni, L., Speiser, D.E., Lichterfeld, M., and Bonini, C. (2017). T memory stem cells in health and disease. Nat. Med. *23*, 18–27. https://doi.org/10.1038/nm.4241.

Gattinoni, L., Zhong, X.-S., Palmer, D.C., Ji, Y., Hinrichs, C.S., Yu, Z., Wrzesinski, C., Boni, A., Cassard, L., Garvin, L.M., et al. (2009). Wnt signaling arrests effector T cell differentiation and generates CD8+ memory stem cells. Nat. Med. *15*, 808–813. https://doi.org/10.1038/nm.1982.

Ghosh, S., Haribabu, B., and Jala, V.R. (2021). Microbial metabolite urolithin A induces expansion of Regulatory T cells in aryl hydrocarbon receptor (AhR)-dependent manner. J. Immunol. *206*, 113.03.

Hombach, A., Wieczarkowiecz, A., Marquardt, T., Heuser, C., Usai, L., Pohl, C., Seliger, B., and Abken, H. (2001). Tumor-specific T cell activation by recombinant immunoreceptors: CD3 zeta signaling and CD28 costimulation are simultaneously required for efficient IL-2 secretion and can be integrated into one combined CD28/CD3 zeta signaling receptor molecule. J. Immunol. *167*, 6123–6131. https://doi.org/10.4049/jimmunol.167.11.6123.

Ichii, H., Sakamoto, A., Hatano, M., Okada, S., Toyama, H., Taki, S., Arima, M., Kuroda, Y., and Tokuhisa, T. (2002). Role for Bcl-6 in the generation and maintenance of memory CD8+ T cells. Nat. Immunol. *3*, 558–563. https://doi.org/10.1038/ni802.

Jaganathan, S.K., Vellayappan, M.V., Narasimhan, G., and Supriyanto, E. (2014). Role of pomegranate and citrus fruit juices in colon cancer prevention. World J. Gastroenterol. *20*, 4618–4625. https://doi.org/10.3748/wjg.v20.i16.4618.

June, C.H., O'Connor, R.S., Kawalekar, O.U., Ghassemi, S., and Milone, M.C. (2018). CAR T cell immunotherapy for human cancer. Science *359*, 1361–1365. https://doi.org/10.1126/science.aar6711.

Kratchmarov, R., Magun, A.M., and Reiner, S.L. (2018). TCF1 expression marks self-renewing human CD8+ T cells. Blood Adv. *2*, 1685–1690. https://doi.org/10.1182/bloodadvances.2018016279.

Le, D.T., Uram, J.N., Wang, H., Bartlett, B.R., Kemberling, H., Eyring, A.D., Skora, A.D., Luber, B.S., Azad, N.S., Laheru, D., et al. (2015). PD-1 blockade in tumors with mismatch-repair deficiency. N. Engl. J. Med. *372*, 2509–2520. https://doi.org/10.1056/NEJMoa1500596.

Luan, P., D'Amico, D., Andreux, P.A., Laurila, P.-P., Wohlwend, M., Li, H., Imamura de Lima, T., Place, N., Rinsch, C., Zanou, N., et al. (2021). Urolithin A improves muscle function by inducing mitophagy in muscular dystrophy. Sci. Transl. Med. *13*, eabb0319. https://doi.org/10.1126/scitranslmed.abb0319.

Majzner, R.G., and Mackall, C.L. (2019). Clinical lessons learned from the first leg of the CAR T cell journey. Nat. Med. *25*, 1341–1355. https://doi.org/10.1038/s41591-019-0564-6.

Mo, F., Yu, Z., Li, P., Oh, J., Spolski, R., Zhao, L., Glassman, C.R., Yamamoto, T.N., Chen, Y., Golebiowski, F.M., et al. (2021). An engineered IL-2 partial agonist promotes CD8+ T cell stemness. Nature *597*, 544–548. https://doi.org/10.1038/s41586-021-03861-0.

Nicolas, A.M., Pesic, M., Engel, E., Ziegler, P.K., Diefenhardt, M., Kennel, K.B., Buettner, F., Conche, C., Petrocelli, V., Elwakeel, E., et al. (2022). Inflammatory fibroblasts mediate resistance to neoadjuvant therapy in rectal cancer. Cancer Cell *40*, 168–184.e13. https://doi.org/10.1016/j.ccell.2022.01.004.

Pagès, F., Mlecnik, B., Marliot, F., Bindea, G., Ou, F.-S., Bifulco, C., Lugli, A., Zlobec, I., Rau, T.T., Berger, M.D., et al. (2018). International validation of the

consensus Immunoscore for the classification of colon cancer: a prognostic and accuracy study. Lancet *391*, 2128–2139. https://doi.org/10.1016/S0140-6736(18)30789-X.

Parisi, G., Saco, J.D., Salazar, F.B., Tsoi, J., Krystofinski, P., Puig-Saus, C., Zhang, R., Zhou, J., Cheung-Lau, G.C., Garcia, A.J., et al. (2020). Persistence of adoptively transferred T cells with a kinetically engineered IL-2 receptor agonist. Nat. Commun. *11*, 660. https://doi.org/10.1038/s41467-019-12901-3.

Pfeiffer, A., Thalheimer, F.B., Hartmann, S., Frank, A.M., Bender, R.R., Danisch, S., Costa, C., Wels, W.S., Modlich, U., Stripecke, R., et al. (2018). In vivo generation of human CD19-CAR T cells results in B-cell depletion and signs of cytokine release syndrome. EMBO Mol. Med. *10*, e9158. https://doi.org/10.15252/emmm.201809158.

Pilipow, K., Scamardella, E., Puccio, S., Gautam, S., Paoli, F. de, Mazza, E.M., Simone, G. de, Polletti, S., Buccilli, M., Zanon, V., et al. (2018). Antioxidant metabolism regulates CD8+ T memory stem cell formation and antitumor immunity. JCI Insight *3*, e122299. https://doi.org/10.1172/jci.insight.122299.

Reschke, R., Yu, J., Flood, B., Higgs, E.F., Hatogai, K., and Gajewski, T.F. (2021). Immune cell and tumor cell-derived CXCL10 is indicative of immunotherapy response in metastatic melanoma. J. Immunother. Cancer *9*, e003521. https://doi.org/10.1136/jitc-2021-003521.

Roberto, A., Castagna, L., Zanon, V., Bramanti, S., Crocchiolo, R., McLaren, J.E., Gandolfi, S., Tentorio, P., Sarina, B., Timofeeva, I., et al. (2015). Role of naive-derived T memory stem cells in T-cell reconstitution following allogeneic transplantation. Blood *125*, 2855–2864. https://doi.org/10.1182/blood-2014-11-608406.

Rosenberg, S.A., and Restifo, N.P. (2015). Adoptive cell transfer as personalized immunotherapy for human cancer. Science *348*, 62–68. https://doi.org/10.1126/science.aaa4967.

Roychoudhuri, R., Clever, D., Li, P., Wakabayashi, Y., Quinn, K.M., Klebanoff, C.A., Ji, Y., Sukumar, M., Eil, R.L., Yu, Z., et al. (2016). BACH2 regulates CD8(+) T cell differentiation by controlling access of AP-1 factors to enhancers. Nat. Immunol. *17*, 851–860. https://doi.org/10.1038/ni.3441.

Ryu, D., Mouchiroud, L., Andreux, P.A., Katsyuba, E., Moullan, N., Nicolet-dit-Félix, A.A., Williams, E.G., Jha, P., Lo Sasso, G., Huzard, D., et al. (2016). Urolithin A induces mitophagy and prolongs lifespan in C. elegans and increases muscle function in rodents. Nat. Med. *22*, 879–888. https://doi.org/10.1038/nm.4132.

Sato, T., Stange, D.E., Ferrante, M., Vries, R.G.J., van Es, J.H., van den Brink, S., van Houdt, W.J., Pronk, A., van Gorp, J., Siersema, P.D., et al. (2011). Long-term expansion of epithelial organoids from human colon, adenoma, adenocarcinoma, and Barrett's epithelium. Gastroenterology *141*, 1762–1772. https://doi.org/10.1053/j.gastro.2011.07.050.

Scharping, N.E., Menk, A.V., Moreci, R.S., Whetstone, R.D., Dadey, R.E., Watkins, S.C., Ferris, R.L., and Delgoffe, G.M. (2016). The tumor microenvironment represses T cell mitochondrial biogenesis to drive intratumoral T cell metabolic insufficiency and dysfunction. Immunity *45*, 374–388. https://doi.org/10.1016/j.immuni.2016.07.009.

Schmitt, M., and Greten, F.R. (2021). The inflammatory pathogenesis of colorectal cancer. Nat. Rev. Immunol. *21*, 653–667. https://doi.org/10.1038/s41577-021-00534-x.

Schnalzger, T.E., Groot, M.H. de, Zhang, C., Mosa, M.H., Michels, B.E., Röder, J., Darvishi, T., Wels, W.S., and Farin, H.F. (2019). 3D model for CAR-mediated cytotoxicity using patient-derived colorectal cancer organoids. EMBO J. *38*, e100928. https://doi.org/10.15252/embj.2018100928.

Scholz, G., Jandus, C., Zhang, L., Grandclément, C., Lopez-Mejia, I.C., Soneson, C., Delorenzi, M., Fajas, L., Held, W., Dormond, O., et al. (2016). Modulation of mTOR signalling triggers the formation of stem cell-like memory T cells. EBioMedicine *4*, 50–61. https://doi.org/10.1016/j.ebiom.2016.01.019.

Schumann, J., Stanko, K., Schliesser, U., Appelt, C., and Sawitzki, B. (2015). Differences in CD44 surface expression levels and function discriminates IL-17 and IFN-γ producing helper T cells. PLoS One *10*, e0132479. https://doi.org/10.1371/journal.pone.0132479.

Schwank, G., and Clevers, H. (2016). CRISPR/Cas9-mediated genome editing of mouse small intestinal organoids. Methods Mol. Biol. *1422*, 3–11. https://doi.org/10.1007/978-1-4939-3603-8_1.

Seeram, N.P., Adams, L.S., Henning, S.M., Niu, Y., Zhang, Y., Nair, M.G., and Heber, D. (2005). In vitro antiproliferative, apoptotic and antioxidant activities of punicalagin, ellagic acid and a total pomegranate tannin extract are enhanced in combination with other polyphenols as found in pomegranate juice. J. Nutr. Biochem. *16*, 360–367. https://doi.org/10.1016/j.jnutbio.2005.01.006.

Shen, P.-X., Li, X., Deng, S.-Y., Zhao, L., Zhang, Y.-Y., Deng, X., Han, B., Yu, J., Li, Y., Wang, Z.-Z., et al. (2021). Urolithin A ameliorates experimental autoimmune encephalomyelitis by targeting aryl hydrocarbon receptor. EBiomedicine *64*, 103227. https://doi.org/10.1016/j.ebiom.2021.103227.

Sung, H., Ferlay, J., Siegel, R.L., Laversanne, M., Soerjomataram, I., Jemal, A., and Bray, F. (2021). Global cancer statistics 2020: GLOBOCAN estimates of incidence and mortality worldwide for 36 cancers in 185 countries. CA Cancer J. Clin. *71*, 209–249. https://doi.org/10.3322/caac.21660.

Toney, A.M., Fox, D., Chaidez, V., Ramer-Tait, A.E., and Chung, S. (2021). Immunomodulatory role of urolithin A on metabolic diseases. Biomedicines *9*, 192. https://doi.org/10.3390/biomedicines9020192.

Totiger, T.M., Srinivasan, S., Jala, V.R., Lamichhane, P., Dosch, A.R., Gaidarski, A.A., Joshi, C., Rangappa, S., Castellanos, J., Vemula, P.K., et al. (2019). Urolithin A, a novel natural compound to target PI3K/AKT/mTOR pathway in pancreatic cancer. Mol. Cancer Ther. *18*, 301–311. https://doi.org/10.1158/1535-7163.MCT-18-0464.

Utzschneider, D.T., Charmoy, M., Chennupati, V., Pousse, L., Ferreira, D.P., Calderon-Copete, S., Danilo, M., Alfei, F., Hofmann, M., Wieland, D., et al. (2016). T cell factor 1-expressing memory-like CD8(+) T cells sustain the immune response to chronic viral infections. Immunity *45*, 415–427. https://doi.org/10.1016/j.immuni.2016.07.021.

van de Wetering, M., Francies, H.E., Francis, J.M., Bounova, G., Iorio, F., Pronk, A., van Houdt, W., van Gorp, J., Taylor-Weiner, A., Kester, L., et al. (2015). Prospective derivation of a living organoid biobank of colorectal cancer patients. Cell *161*, 933–945. https://doi.org/10.1016/j.cell.2015.03.053.

van den Eynde, M., Mlecnik, B., Bindea, G., Fredriksen, T., Church, S.E., Lafontaine, L., Haicheur, N., Marliot, F., Angelova, M., Vasaturo, A., et al. (2018). The link between the multiverse of immune microenvironments in metastases and the survival of colorectal cancer patients. Cancer Cell *34*, 1012–1026.e3. https://doi.org/10.1016/j.ccell.2018.11.003.

Vannini, N., Campos, V., Girotra, M., Trachsel, V., Rojas-Sutterlin, S., Tratwal, J., Ragusa, S., Stefanidis, E., Ryu, D., Rainer, P.Y., et al. (2019). The NAD-booster nicotinamide riboside potently stimulates hematopoiesis through increased mitochondrial clearance. Cell Stem Cell *24*, 405–418.e7. https://doi.org/10.1016/j.stem.2019.02.012.

Varga, J., Nicolas, A., Petrocelli, V., Pesic, M., Mahmoud, A., Michels, B.E., Etlioglu, E., Yepes, D., Häupl, B., Ziegler, P.K., et al. (2020). AKT-dependent NOTCH3 activation drives tumor progression in a model of mesenchymal colorectal cancer. J. Exp. Med. *217*, e20191515. https://doi.org/10.1084/jem.20191515.

Verma, V., Jafarzadeh, N., Boi, S., Kundu, S., Jiang, Z., Fan, Y., Lopez, J., Nandre, R., Zeng, P., Alolaqi, F., et al. (2021). MEK inhibition reprograms CD8+ T lymphocytes into memory stem cells with potent antitumor effects. Nat. Immunol. *22*, 53–66. https://doi.org/10.1038/s41590-020-00818-9.

Weidner, T., Agarwal, S., Perian, S., Fusil, F., Braun, G., Hartmann, J., Verhoeyen, E., and Buchholz, C.J. (2021). Genetic in vivo engineering of human T lymphocytes in mouse models. Nat. Protoc. *16*, 3210–3240. https://doi.org/10.1038/s41596-021-00510-8.

Xiong, Y., Wang, L., Di Giorgio, E., Akimova, T., Beier, U.H., Han, R., Trevisanut, M., Kalin, J.H., Cole, P.A., and Hancock, W.W. (2020). Inhibiting the coregulator CoREST impairs Foxp3+ Treg function and promotes antitumor immunity. J. Clin. Invest. *130*, 1830–1842. https://doi.org/10.1172/JCI131375.

Yamaguchi, A., Ishikawa, H., Furuoka, M., Yokozeki, M., Matsuda, N., Tanimura, S., and Takeda, K. (2019). Cleaved PGAM5 is released from

mitochondria depending on proteasome-mediated rupture of the outer mitochondrial membrane during mitophagy. J. Biochem. *165*, 19–25. https://doi.org/10.1093/jb/mvy077.

Yu, B., Ma, J., Li, J., Wang, D., Wang, Z., and Wang, S. (2020a). Mitochondrial phosphatase PGAM5 modulates cellular senescence by regulating mitochondrial dynamics. Nat. Commun. *11*, 2549. https://doi.org/10.1038/s41467-020-16312-7.

Yu, Y.-R., Imrichova, H., Wang, H., Chao, T., Xiao, Z., Gao, M., Rincon-Restrepo, M., Franco, F., Genolet, R., Cheng, W.-C., et al. (2020b). Disturbed mitochondrial dynamics in CD8+ TILs reinforce T cell exhaustion. Nat. Immunol. *21*, 1540–1551. https://doi.org/10.1038/s41590-020-0793-3.

Zhou, X., Yu, S., Zhao, D.-M., Harty, J.T., Badovinac, V.P., and Xue, H.-H. (2010). Differentiation and persistence of memory CD8(+) T cells depend on T cell factor 1. Immunity *33*, 229–240. https://doi.org/10.1016/j.immuni.2010.08.002.

Ziegler, P.K., Bollrath, J., Pallangyo, C.K., Matsutani, T., Canli, Ö., Oliveira, T. de, Diamanti, M.A., Müller, N., Gamrekelashvili, J., Putoczki, T., et al. (2018). Mitophagy in intestinal epithelial cells triggers adaptive immunity during tumorigenesis. Cell *174*, 88–101.e16. https://doi.org/10.1016/j.cell.2018.05.028.

STAR★METHODS

KEY RESOURCES TABLE

REAGENT or RESOURCE	SOURCE	IDENTIFIER
Antibodies		
CD3 (IHC)	Dako	Cat# IS503; RRID:AB_2732001
Gapdh	Santa Cruz	Cat# sc-32233; RRID:AB_627679
Parkin	Santa Cruz	Cat# sc32282; RRID:AB_628104
TOM20	CellSignaling	Cat# 42406S; RRID:AB_2687663
pStat1	CellSignaling	Cat# 9167; RRID:AB_561284
Phospho-β-Catenin	CellSignaling	Cat# 9561; RRID:AB_331729
PGAM5	Abcam	Cat# ab126534; RRID:AB_11127076
β-Actin	Sigma	Cat# A4700; RRID:AB_476730
InvivoMab anti-mouse CD8	Hoelzel	Cat# BE0061; RRID:AB_1125541
InvivoMab rat IgG2b isotype	Hoelzel	Cat# BE0090; RRID:AB_1107780
nVivoMAb anti-mouse PD-1	Hoelzel	Cat# BE0146; RRID:AB_10949053
InVivoMab mouse IgG2b isotype control	Hoelzel	Cat# BE0086; RRID:AB_1107791
anti-human CD3	Miltenyi Biotec	Cat# 130-093-387; RRID:AB_1036144
anti-human CD28	Miltenyi Biotec	Cat# 130-093-375; RRID:AB_1036134
anti-mouse CD3	Biolegend	Cat# 100339; RRID:AB_1115078
anti-mouse CD28	Biolegend	Cat# 102115; RRID:AB_11150408
PerCP/Cyanine5.5 anti-mouse H-2Kb Antibody	BioLegend	Cat# 116516; RRID:AB_1967133
αCEACAM5-APC	R&D Systems	Cat# FAB41281A; RRID:AB_2077589
Fixable Viability Dye-eF780	eBioscience	Cat# 65-0865-14
αCD45-FITC	eBioscience	Cat# 11-0451-85; RRID:AB_465051
αCD11b-BV650	BD	Cat# 56340; RRID:AB_2738184
αCD11c-BV785	BD	Cat# 563735; RRID:AB_2738394
αLy6G-BV605	BD	Cat# 563005; RRID:AB_2737946
αLy6C-AF700	Biolegend	Cat# 128024; RRID:AB_10643270
αF4/80-PE	eBioscience	Cat# 12-4801-82; RRID:AB_465923
αPD-L1-PECy7	eBioscience	Cat# 25-5982-80; RRID:AB_2573508
αCD45-BV786	BD	Cat# 564225; RRID:AB_2716861
αCD4-BUV496	BD	Cat# 564667; RRID:AB_2722549
αCD8-BV605	Biolegend	Cat# 100744; RRID:AB_2562609
αPD1-APC	eBioscience	Cat# 17-9985-82; RRID:AB_11149358
αTIM-3-PECy7	Biolegend	Cat# 119715; RRID:AB_2571932
αCTLA4-PE	Biolegend	Cat# 106305; RRID:AB_313254
αLag3-BV421	Biolegend	Cat# 125221; RRID:AB_2572080
αCD4-FITC	BD	Cat# 553650; RRID:AB_394970
αCD8-APC	eBioscience	Cat# 17-0081-83; RRID:AB_469336
αCD44-AF400	Biolegend	Cat# 103026; RRID:AB_493713
αCD62L-BV785	Biolegend	Cat# 104440; RRID:AB_2629685
αSca-1-PerCP-Cy5.5	eBioscience	Cat# 45-5981-82; RRID:AB_914372
αCD95-PE	BD	Cat# 554258; RRID:AB_395330
αCD8-BV650	BD	Cat# 563234; RRID:AB_2738084
αCD4-BUV496	BD	Cat# 564667; RRID:AB_2722549
αCD127-APC	eBioscience	Cat# 17-1271-82; RRID:AB_469435
αCD95-FITC	Biolegend	Cat# 152605; RRID:AB_2632900
αTCF1-PE	BD	Cat# 564217; RRID:AB_2687845

(*Continued on next page*)

Continued

REAGENT or RESOURCE	SOURCE	IDENTIFIER
αPGC-1α	SantaCruz	Cat# sc-518025; RRID:AB_2890187
αCyclinD1-PE	Invitrogen	Cat# MA5-28534; RRID:AB_2745493
αCD8-PeCy7	Biolegend	Cat# 100722; RRID:AB_312761
αCD4-AF700	Biolegend	Cat# 100429; RRID:AB_493698
αGranzyme B-FITC	Biolegend	Cat# 515403; RRID:AB_2114575
αIFNγ-PerCP-Cy5.5	eBioscience	Cat# 45-7311-82; RRID:AB_1107020
αTNFa-BV711	BD	Cat# 563944; RRID:AB_2738499
αHuman CD95-BV421	BD	Cat# 562616; RRID:AB_2737679
αHuman CD62L-PE	BD	Cat# 555544; RRID:AB_395928
αHuman CCR7-AF700	BD	Cat# 561143; RRID:AB_10562031
αHuman CD45RO-APC	BD	Cat# 559865; RRID:AB_398673
αHuman CD45RA-FITC	BD	Cat# 555488; RRID:AB_395879
αHuman CD8-PE-CF594	BD	Cat# 562282; RRID:AB_11154052
αHuman CD4-BV786	BD	Cat# 566806; RRID:AB_2869878
αHuman αCD45RA-VioBlue	Miltenyi	Cat# 130-113-922; RRID:AB_2726409
αHuman αmycCAR-FITC	Miltenyi	Cat# 130-116-653; RRID:AB_2751329
αHuman CD8- PerCP-Cy5.5	BD	Cat# 560662; RRID:AB_1727513
αHuman CD62L-PE-Vio770	Miltenyi	Cat# 130-113-621; RRID:AB_2751151
αHuman CD45RO-APC	Miltenyi	Cat# 130-113-546; RRID:AB_2733383
anti-rabbit IgG Alexa Fluor 488	ThermoFisher Scientific	Cat# A-11008; RRID:AB_143165
Biological samples		
APTK mouse organoids	Nicolas et al., 2022	N/A
Human leukocytes	This study	N/A
Human CRC organoids	This study	N/A
APTK-OVA mouse organoids	This study	N/A
Chemicals, peptides, and recombinant proteins		
Urolithin A	Tocris	Cat# 6762
Advanced DMEM F12	ThermoFisher Scientific	Cat# 12634010
Fetal bovine serum	Thermo Fisher Scientific	Cat# 10500056
Accutase cell dissociation reagent	ThermoFisher Scientific	Cat# A1110501
Glutamax	ThermoFisher Scientific	Cat# 35050061
HEPES	ThermoFisher Scientific	Cat# 15630080
Penicillin/ Streptomycin	ThermoFisher Scientific	Cat# 15070063
B-27 supplement	ThermoFisher Scientific	Cat# 12587010
N-2 supplement	ThermoFisher Scientific	Cat# 17502048
N-Acetylcysteine	Sigma-Aldrich	Cat# A9165
SB202190	BioTrend	Cat# HY-10295-50mg
Human EGF	PeproTech	Cat# AF-100-15
Matrigel	Corning	Cat# 356231
Cultrex Basement Membrane Extract, Type 2	RnD Systems	Cat# 3532-005-02P
EDTA	ThermoFisher Scientific	Cat# AM9260G
Puromycin dihydrochloride	Merck	Cat# 58-58-2
SuperScriptII Reverse Transcriptase	Invitrogen	Cat# 18064-014
SYBR Green Master Mix	Roche	Cat# 04913914001
OligoDT	Invitrogen	Cat# N8080128
DNTP	Invitrogen	Cat# AM8200
Ribonuclease inhibitor RNAseOUT	Invitrogen	Cat# 10777019
LysoTracker red DND-99	Thermo Fisher Scientific	Cat# L7528
MitoTracker deep red	Thermo Fisher Scientific	Cat# M22426

(*Continued on next page*)

Continued

REAGENT or RESOURCE	SOURCE	IDENTIFIER
Mitoprobe TMRM kit	Thermo Fisher Scientific	Cat# M20036
Qiagen RNeasy Mini kit	Qiagen	Cat# 74106
Cell Fractionation Kit	Abcam	Cat# Ab109719
Pierce™ Coomassie Plus (Bradford) Assay Reagent	Thermo Fisher Scientific	Cat# 23236
Phorbol 12-myristate 13-acetate	Sigma	Cat# P8139
Polyethylenimine	Sigma-Aldrich	Cat# 408727-100ML
Ionomycin	Sigma	Cat# I3909
Azoxymethane	Sigma	Cat# A5486
Brefeldin A	BioLegend	Cat# 420601
Live/Dead Fixable Blue Dead Cell Stain Kit	Thermo Fisher Scientific	Cat# L23105
Transcription factor buffer set	BD Biosciences	Cat# 562574
Cytofix/Cytoperm	BD Biosciences	Cat# 554714
RPMI 1640	Sigma	Cat# R0883
4Cell® Nutri-T media	Sartorius	Cat# 05-11F2001-1K
Glutamine	Sigma	Cat# G7513
αCD3/CD28 activation beads mouse	ThermoFisher Scientific	Cat# 11456D
αCD3/CD28 activation beads human	ThermoFisher Scientific	Cat# 11131D
EasySep Mouse T cell Isolation Kit	StemCell	Cat# 19851
EasySep Human T Cell Kit	StemCell	Cat# 17951
CellTrace Violet	Thermo Fisher Scientific	Cat# C34557
ICG-001	SelleckChem	Cat# S2662
SR-18292	Sigma-Aldrich	Cat# SML2146
Ficoll Paque	GE healthcare	Cat# 11768538
Human IL-7	Miltenyi Biotec	Cat# 130-095-362
Human IL-15	Miltenyi Biotec	Cat# 130-095-765
ONE-Glo™ EX Luciferase Assay System	Promega	Cat# E8110
Tumor & Tissue Dissociation Reagent	BD Horizon	Cat# 661563
ProLong™ Gold Antifade Mountant	ThermoFisher	Cat# P36930
Urolithin A diet	Brogaarden	N/A
AIN-93G control food	Brogaarden	N/A
Deposited data		
T cell Urolithin A and DMSO stimulation RNA-seq	This study	NCBI-GEO: GSE213562
Experimental models: Cell lines		
HEK293T cells	ATCC	Cat# CRL-11268
Nalm-6 cells	ATCC	Cat# CRL-3273
Human CRC organoids	This study	N/A
Experimental models: Organisms/strains		
Mouse: C57BL/6J	Janvier Labs	N/A
Mouse: FVB/NRj	Janvier Labs	N/A
Mouse: B6.129S7-Rag1tm1Mom/J	The Jackson Laboratories	Strain #:002216: RRID:IMSR_JAX:002216
Mouse: OT-I: Tg(TcraTcrb)1100Mjb	The Jackson Laboratories	Strain#003831; RRID:MGI:5292730
Mouse: B6.129S4-Pink1tm1Shn/J	The Jackson Laboratories	Strain #:017946; RRID:IMSR_JAX:017946
Mouse: Pgam5-/-	Gift from Christoph Becker	N/A
Oligonucleotides		
Table S1. List of human qRT_PCR primers		
Recombinant DNA		
pMD2.G plasmid	Addgene	Addgene 12259
pS-CD19.CAR-W plasmid	Pfeiffer et al., 2018	N/A

(*Continued on next page*)

Continued

REAGENT or RESOURCE	SOURCE	IDENTIFIER
pCMVdR8.9 plasmid	Pfeiffer et al., 2018	N/A
Software and algorithms		
Aperio ImageScope 12.4	Leicabiosystems	N/A
ImageJ Software	Open source	N/A
Ingenuity Pathway Analysis Software	Qiagen	N/A
GraphPad Prism 8	GraphPad	N/A
FlowJo V10	BD	N/A

RESOURCE AVAILABILITY

Lead contact

Further information and requests for resources and reagents should be directed to and will be fulfilled by the lead contact, Florian R. Greten.

Materials availability

This study did not generate new unique reagents.

Data and code availability

- Total RNA sequencing data of UA/DMSO-treated T-cells during this study are available at: NCBI-GEO: GSE213562. Flow cytometry gating strategies are included in the Supplementary Figures.
- This paper does not report original code.
- Any additional information required to reanalyze the data reported in this paper is available from the lead contact upon request.

EXPERIMENTAL MODEL AND SUBJECT DETAILS

Mice

Mice aged 6-30 weeks were maintained in a temperature controlled room with 12 h light and 12 h dark diurnal cycle. They were housed in filter-topped cages and fed standard laboratory chow and water ad libitum unless indicated otherwise. All animal procedures were performed in accordance with institutional guidelines. FvB and C57BL/6J mice were ordered from CharlesRiver and Janvier, while *Rag1*$^{-/-}$ and OT-1 mice were bred in-house. *Pink1*$^{-/-}$ mice (B6.129S4-Pink1tm1Shn/J; Strain #:017946) were purchased from The Jackson Laboratory. *Pgam5*$^{-/-}$ mice were a gift from C.B.

Urolithin A containing diet (2,28g/kg) or AIN-93G control food (Brogaarden) were given *ad libitum* once introduced for experimental purpose at the indicated time. Animal experiments were approved by the Regierungspräsidium Darmstadt under animal application numbers F123/1009; F123/1062 and F123/2008.

Human samples

Human leukocytes were obtained from venous blood of mixed-sex donors aged 25-45 years after informed consent. CRC organoids were generated as part of the interdisciplinary Biobank and Database Frankfurt (iBDF) after prior written informed consent. The study was approved by the institutional review board of the UCT and the Ethical Committee at the University Hospital Frankfurt (Ethics vote: 4/09; project-numbers: SGI-06-2015 and SGI-17-2020).

METHOD DETAILS

In vitro T cell isolation and stimulation

Splenic murine T cells were isolated from mice aged 6-20 weeks by negative selection with EasySep mouse T cell isolation kit (Stem cell) according to the manufacturer's instructions. To monitor T cell proliferation, purified T cells were loaded with CellTrace Violet (C34557 ThermoFisher Scientific). T cell activation was initiated using αCD3/CD28 activation beads (11456D; ThermoFisher Scientific) at a ratio of 25μl dynabeads per 0,5x10^6 T-cells. Cells were activated with 25-50 μM Urolithin A (Tocris) or DMSO in T cell activation Medium (RPMI (ThermoFisher Scientific) 10% FBS (South America origin), 10mM Hepes (Sigma), 1x Non-Essential Amino Acid, 1mM Sodium Pyruvate, 50μM β-Mercaptoethanol, 100 U/ml penicillin, 100 μg/ml streptomycin and 2mM Glutamax (ThermoFisher Scientific) for the indicated durations. In selected experiments, cells were stimulated in the presence of inhibitors, namely TCF1i (ICG-001; SelleckChem; 10μM) and PGC-1αi (SR-18292, Sigma-Aldrich; 10μm,). For subsequent analysis, activating beads were magnetically removed prior antibody staining. For human T cells, peripheral blood mononuclear cells were purified with a Ficoll-Paque (GE healthcare) gradient. T cells were enriched with EasySep Human T Cell Isolation Kit (StemCell) and activated with

dynabead Human T-Activator CD3/CD28 for T Cell Expansion and Activation Kit (11131D; ThermoFisher Scientific), similar to murine T cell stimulation.

When the subsequent activation and expansion of CAR T cells was studied, plates were coated with 1 μg/mL anti-human CD3 (aCD3; clone OKT3) and thawed PBMC were cultivated with 3 μg/mL anti-human CD28 (aCD28; 15E8, both Miltenyi Biotec) containing media for three days. (NutriT media (4Cell® Nutri-T media (Sartorius) containing 0.5% penicillin/streptomycin) supplemented with IL-7 (25 U/ml) and IL-15 (U/ml) (all Miltenyi Biotec).

Organoids

APTK colorectal organoids which harbor mutations for *Apc*, *Trp53* and *Tgfbr2* as well as expression of oncogenic $Kras^{G12D}$ were established and maintained as previously described (Nicolas et al., 2022; Varga et al., 2020). APTK organoids were seeded in 6 wells suspension plates: 6 droplets of 50 μl Matrigel (Corning) per well were used. To generate OVA-APTK, colon organoids were isolated from unchallenged OVA mice (The Jackson Laboratory) as previously described (Nicolas et al., 2022). Liposomes CRISPR/Cas9 technology- based transfection was used for targeted knockout of the following mutated colorectal cancer-related genes: *Apc* (gRNA: TATGGAACCTGTCTGCACACTGCAC), *Trp53* gRNA: GACACTCGGAGGGCTTCACT) and *Tgfbr2* (gRNA: GGCCGCTGCA TATCGTCCTG) as previously described (Schwank and Clevers, 2016). Cas9 plasmid (Addgene; #41815) was used along gRNA plasmids generated from addgene #41819 plasmid by cloning the gRNA of interest instead of GFP targeting gRNA. Firstly, *Apc* knockout (A) organoids were functionally selected by the withdrawal of R-spondin from the culture medium. Secondly, *Apc Trp53* (AT) knockout organoids were selected for *Trp53* loss with 5 μM of MDM2 inhibitor (Nutlin-3) (Biomole, cat no. 10004372). Thirdly, *Apc Trp53 Tgfbr2* (APT) knockout organoids were selected with 5 μM recombinant TGFβ (R&D Systems; 7666-MB). Finally, $Kras^{G12D}$ gain of function mutation was obtained by overexpressing the active murine version of *Kras* gene (cloned in house based on Addgene plasmid #111164, Map-S5) in APT organoids. *Apc*, *Trp53*, *Tgfbr2* and $Kras^{G12D}$ (APTK) OVA organoids were selected by 2 μg/mL puromycin (Merck; 58-58-2) and withdrawal of EGF and noggin from the culture medium. In order to study the effect of UA on lysosome formation, mitochondria reduction as well as antigen presentation, organoids were treated with 25-50 μM UA for 24-48h. Organoids were subsequently stained with a MHC-I antibody (AF6-88.5; 116516; BioLegend), Mitotracker Deep Red (250nm; ThermoFisher) and Lysotracker Red DND-99 (75nM; ThermoFisher).

Human CRC organoids were established and cultured as previously described (Sato et al., 2011; van de Wetering et al., 2015). Organoids were cultured in medium composed of advanced DMEM/F12 supplemented with 20% R-spondin CM, 10% Noggin CM, 10 mM HEPES, 1× GlutaMax, 1× penicillin/streptomycin, 2% B27, 10 mM nicotinamide (Sigma-Aldrich), 12.5 mM N-acetylcystein (Sigma-Aldrich), 500 nM A83-01 (Tocris), 10 μM SB202190 (Biotrend), and 50 ng/ml human EGF (PeproTech). Unless stated otherwise, all media components were purchased from Life Technologies.

Cell culture

Nalm-6 cells were cultivated in RPMI 1640 (Sigma, R0883-500 mL) medium supplemented with 10% fetal bovine serum (FBS; Sigma, F7524) and 2 mM glutamine (Sigma, G7513-100 ml). Their identity was confirmed by genetic phenotyping performed by the German cell culture collection (DSMZ).

Colorectal cancer models

Colorectal tumors were induced by 6 consecutive weekly injections of AOM on mice fed with food containing 2,28g/kg Urolithin A (UA diet) or with control food. The diet was introduced one-week prior the first AOM injection and maintained until the end of the experiment at ~20-24 weeks. The colons were collected for subsequent histological analysis as described below.

For subcutaneous colorectal cancers, APTK organoids were mechanistically disrupted, incubated with Accutase to generate a single cell suspension and reconstituted in PBS 20% Matrigel (Corning) for subcutaneous transplantation. Tumor sizes were measured at the indicated time after transplantation and tumor volume quantified as ½(width^2 x length). Urolithin A or control food regiment were initiated either one week before tumor challenge or 11 days after tumor development. Therapeutic diets were maintained throughout the experiment unless indicated otherwise. 200μg CD8-depleting antibodies (InvivoMab anti-mouse CD8; Hoelzel; BE0061) or isotype controls (InvivoMab rat IgG2b isotyp; Hoelzel; BE0090) were applied every three days, starting at five days after tumor initiation. To study combination efficacy with immunotherapy, mice were injected i.p. with 100μl nVivoMAb anti-mouse PD-1(Hoelzel; BE0146) and InVivoMab mouse IgG2b isotype control (Hoelzel; BE0086) every 2 days, starting three days after tumor injection.

Adoptive cell transfer

For adoptive cell transfer transfer, purified splenic T cell from OT1 mice were isolated and activated using αCD3/aCD28 stimulation beads for 48h. After magnetic bead removal, 1x10^6 T of activated T cell were intravenously injected into $Rag1^{-/-}$ recipients. To study survival of transferred T cells, stimulated OT-1 T cells were injected into mice without tumors. Subsequently, after 7 days, spleens were isolated and splenocytes were stained for the $CD8^+$ subsets as described below. To understand antitumor immunity conferred by transferred OT-1 lymphocytes, cells were injected into mice carrying APTK-OVA tumors 10 days after subcutaneous organoid transplantation. Tumor growth was assessed as described above. Mice were kept under regular chow food for the T cell adoptive transfer experiment and sacrificed collectively when maximum tumor diameter extended 1,5 cm.

Lentiviral (LV) production

Lentiviral vectors (LVs) were produced as described previously in detail for receptor targeted LVs (Weidner et al., 2021). In brief, HEK293T cells (ATCC CRL-11268) were transfected with a VSVG envelope (pMD2.G, Addgene: 12259), transfer and packaging plasmid in a ratio of 35:100:65 in presence of polyethylenimine (PEI; Sigma-Aldrich, 408727-100ML). The transfer vector plasmids encoded second generation CARs. The CEA-CAR encoding plasmid (Hombach et al., 2001) was modified by inserting the coding sequence for the reporter ΔLNGFR. The CD19-CAR contains a myc-tag for detection and was described (Pfeiffer et al., 2018). LVs were harvested from culture supernatants 48h after transfection, concentrated by a 24h centrifugation through a 20% sucrose cushion (Sigma, 84097) at 4,500 × g (4°C), and re-suspended in Dulbecco's phosphate-buffered saline (DPBS, Mg2+ and Ca2+ free; Biowest, L0615-500). LVs were stored at -80°C and thawed only once for each experimental use.

CAR gene delivery

For transduction, fully activated PBMC were seeded at $8x10^4$ cells/well in NutriT media supplemented with IL-7 and IL-15 in a 96-well plate. 0.5 μL VSV-LV was added to the cells, following spinfection via centrifugation for 90 min at 850xg and 32°C. After spinfection, 100 μL of fresh media was added. Optionally, medium was replaced with fresh medium containing 25 μM UA or DMSO 5 h post incubation with VSV-LV. Subsequently, cells were further cultivated at 37°C. Three days post transduction, CD19 CAR expression and the amount of T_{SCM} were determined. For CEA CAR T cells, T cells were frozen upon transduction and thawed for UA exposure experiments.

CAR T cell killing assay

The cytotoxic activity of CD19-CAR T cells generated in presence or absence of UA was determined by CD19-positive Nalm-6 cell killing. Three days post transduction, CAR expression was determined and normalized to equal CAR T cell levels. Cells were washed twice and $0.5x10^4$ CAR T cells were seeded into NutriT medium without cytokines, UA or DMSO. Nalm-6 cells were labeled using CellTrace™ Violet (CTV; Thermo Fisher Scientific, C34557) following manufacturer's instructions and $1x10^4$ labeled Nalm-6 cells were added to the CAR T cells (0.5:1 effector to target ratio). The amount of dead target cells was determined via flow cytometry 24 h after start of killing.

In human CRC organoids, CEA-expression was confirmed by flow cytometry αCEACAM5-APC (487609; FAB41281A; R&D Systems) Before co-culture, CEA-CAR T cells were cultivated in presence or absence of UA for three days. The cytotoxicity assay was performed as described (Schnalzger et al., 2019), using 96 well plates coated with 15 μl Cultrex Basement Membrane Extract, Type 2 per well and organoids were seeded at a ratio of 1:8. Co-culture was performed for three days with $0.5x10^4$ CAR T cells per well resuspended in organoid medium (as described above) without IL-7/IL-15. 100 μl luciferase assay reagent composed of 10% One-Glo EX Reagent (Promega) in lysis buffer (50 mM NaCl, 50 mM Tris–HCl pH 7.4, 1% Triton X-100) was added to each well and incubated at room temperature for 1h protected from light. 100 μl of each sample was transferred to an opaque 96-well microtiter plate and measured using a SpectraMax iD3 microplate reader (Molecular Devices).

For freezing of CAR-T cells, pelleted cells were resuspended in 500μl of NutriT medium supplemented with 20% FCS. 500 μl of NutriT medium supplemented with 20% FCS and 20% DMSO was added dropwise. For thawing, a vial of CAR T cells heated for 1 min in a 37°C water bath. Thawed cells were washed twice with NutriT medium, centrifuged (5min, 330 g) and resuspended in NutriT medium supplemented with IL-7 (25 U/ml) and IL-15 (U/ml).

Tumor collection and sample preparation

Tumors were minced and digested with Tumor & Tissue Dissociation Reagent (BD Horizon) for 30 min. The remaining organ pieces were filtered through a 70 μm cell strainer. Cells were then washed with PBS 1% BSA and 2mM EDTA. Immune cells were enriched on a 30%/40%/75% Percoll gradient after a 1700 rpm 17 min centrifugation. Then, tumor immune filtrates or activated T cells were stained with Fixable Viability Dye-eF780 (65-0865-14; eBioscience), αCD45-FITC (30-F11; 11-0451-85; eBioscience), αCD11b-BV650 (M1/70; 56340; BD) α-CD11c-BV785 (HL3; 563735; BD), αLy6G-BV605 (53-6.7; 563005; BD), αLy6C-AF700 (HK1.4; 128024; Biolegend), αF4/80-PE (BM8; 12-4801-82, eBioscience), αPD-L1-PECy7 (MIH5; 25-5982-80, eBioscience); or with Fixable Viability Dye-eF780 (ebioscience), αCD45-BV786 (30-F11; 564225; BD), αCD4-BUV496 (GK1.5; 564667; BD), αCD8-BV605 (100744; Biolegend), αPD1-APC (J43; 17-9985-82; eBioscience), αTIM-3-PECy7 (RMT3-23; 119715; Biolegend), αCTLA4-PE (UC10-4B9; 106305; Biolegend) and αLag3-BV421 (C9B7W; 125221, Biolegend); or with Fixable Viability Dye-eF780 (eBioscience), αCD4-FITC (H129.19; 553650; BD), αCD8-APC (53-6.7; 17-0081-83; eBioscience), αCD44-AF400 (IM7; 103026; Biolegend), αCD62L-BV785 (MEL-14; 104440; Biolegend), αSca-1-PerCP-Cy5.5 (D7; 45-5981-82; eBioscience), αCD95-PE (Jo2; 554258; BD); or with Fixable Viability Dye-eF780 (eBioscience), αCD8-BV650 (53-6.7; 563234; BD), αCD4-BUV496 (GK1.5; 564667; BD), αCD127-APC (A7R34; 17-1271-82; eBioscience), αCD95-FITC (SA367H8;152605; Biolegend), αCD44-AF400 (IM7; 103026; Biolegend), αCD62L-BV785 (MEL-14; 104440; Biolegend), αSca-1-PerCP-Cy5.5 (D7; 45-5981-82; eBioscience) followed by intracellular staining of αTCF1-PE (S33-966; 564217; BD), or PGC-1α (sc-518025; D-5; santa cruz), or αCyclinD1 (MA5-28534, DCS-6; Invitrogen) with transcription factor buffer set kit (BD Biosciences). To study cytokine expression, tumor immune infiltrates were stimulated *ex vivo* with 20ng/ml PMA and 1μg/ml Ionomycin (Sigma) for 3h in T cell activation medium with Brefeldin A (Biolegend). For T cell *in vitro* activation experiments over several days, Brefeldin A was added to the medium for the last 3 hours. Cells were then stained with Fixable Viability Dye-eF780 (eBioscience), αCD8-PeCy7 (53.6-7; 100722; Biolegend), αCD4-AF700 (GK1.5; 100429; Biolegend), and intracellular staining for cytokine assessment was performed with BD Cytofix/Cytoperm (BD) with 20 min fixation and overnight

incubation with αGranzyme B-FITC (GB11; 515403; Biolegend), αIFNγ-PerCP-Cy5.5 (XMG1.2; 45-7311-82; eBioscience) and αTNFa-BV711 (MP6-XT22; 563944; BD).

For flow cytometric analysis of mitochondria and lysosomes 500μl of Mitotracker Red (200nM; ThermoFisher) or Lysotracker Red DND-99 (75nM; Thermo Fisher) were applied followed by surface staining. To study changes in mitochondrial membrane potential, Mitoprobe TMRM kit (Thermo Fisher) was used according to the manufacturer's instructions. Cell proliferation was assessed by CellTrace Violet (Invitrogen, C34557) at a concentration of 5μM according to manufacturer's instructions. For human samples, cells were stained as described above with Fixable Viability Dye-eF780, αCD95-BV421 (DX2; 562616), αCD62L-PE (DREG-56; 555544), αCCR7-AF700 (150503; 561143), αCD45RO-APC (UCHL; 559865), αCD45RA-FITC (HI100; 555488), αCD8-PE-CF594 (RPA-T8; 562282) and αCD4-BV786 (OKT4; 566806) from BD.

For experiments studying activation, expansion and exhaustion of CAR T cells, cells were stained with αCD45RA-VioBlue (T6D11; 130-113-922; Miltenyi), αmycCAR-FITC (SH1-26e7.1.3; 130-116-653; Miltenyi), αCD8- PerCP-Cy5.5 (RPA-T8; 560662; BD), CD62L-PE-Vio770 (145/15; 130-113-621; Miltenyi), CD45RO-APC (UCHL1, 130-113-546; Miltenyi), Fixable Viability Dye-eF780; or mycCAR-FITC (SH1-26e7.1.3; 130-116-653; Miltenyi), αCD8- PerCP-Cy5.5 (RPA-T8; 560662; BD), αPD1- PE-Vio770 (PD1.3.1.3; 130-117-810; Miltenyi), αTim3-APC (REA635; 130-119-781; Miltenyi) and Fixable Viability Dye-eF780. Finally, samples were fixed with 1% PFA until data acquisition.

Flow cytometry data acquisition

Cell doublets and cells debris were excluded from the analysis by gating FSC-A vs FSC-H followed by SSC-A vs SSC-H dot plots and FSC-A vs SSC-A dot plots, respectively. eFluor 780 highly positive cells, i.e, dead cells, were gated out of the analysis as well as CD45 negative cells in the case of tumor samples. Data was acquired on Canto II (BD), Fortessa (BD) and Aurora (Cytek) cytometers and analyzed with FlowJo with the subsequent gating strategy described in the supplementary dataset.

Quantitative PCR with reverse transcription analysis

In vitro activated T cells following the indicated treatments were collected followed by RNA isolation using the RNeasy kit (Qiagen). RNA quality and concentration were determined by Nanodrop spectrophotometer. Complementary DNA was generated using SuperScript II reverse transcriptase (ThermoFisher). A total reaction volume of 13 μl RNA was incubated with oligoDT and DNTP Mix (1 μl each) for 5 min at 65°C. The samples were allowed to cool down for 5 min on ice, and to each 4 μl of 5x First strand buffer, 1 μl DTT, 1 μl RNAseOUT™ and 1 μl Superscript II reverse transcriptase were added. Samples were incubated for 1 h at 42°C. Synthesized cDNA was 1:5 diluted in nuclease free water before being processed into gene expression analysis with the 96 wells StepOne real time PCR Machine (Applied biosystems) using 2X FastStart Universal SYBR Green Master Mix (Roche). CT values were normalized to the gene indicated in the respective figures. The following primers were used:

Atg 5 (For: GGAGAGAAGAGGAGCCAGGT, Rev: GCTGGGGGACAATGCTAATA), *Atg7* (For: GCCTAACACAGATGCTGCAA, Rev: TGCTCTTAAACCGAGGCTGT), *Atg12*(For: TAAACTGGTGGCCTCGGAAC, Rev: ATCCCCATGCCTGGGATTTG), *Pik3c3* (For: GTG AAGTACCCTGACCTGCC, Rev: AGTCATGCATTCCTTGGCGA), *p62* (For: GCTGAAGGAAGCTGCCCTAT, Rev: TTGGTCTGTAGGA GCCTGGT), *Bnip3* (For: ATGCACAGCATGAGTCGGG, Rev: CTGGTATGCATCTCAACATCAAACA), *Lamp2* (TGTGCAACAAAGA GCAGGTG, Rev: TCCAGTATGATGGCGCTTGAG), *Pink1* (For: AAGCACCAGAAATTGCGACG, Rev: ACGAGATGGGAGTGCT GGTA), *TCF7* (For: CAATCTGCTCATGCCCTACC, Rev: CTTGCTTCTGCGTGATGTCC), *Rplp0* (For: TTCATTGTGGGAGCAGAC, Rev: CAGCAGTTTCTCCAGAGC), *Lef1* (For: GCAGCTATCAACCAGATCC, Rev GATGTAGGCAGCTGTCATTC), *Axin2* (For: CAGAG GTGGTACCTTGCCAAA, Rev GCCGACAGTGCAAGACCC), *cmyc* (For: AACTACGCAGCGCCTCCC, Rev: ATTTTCGGTTGTTG CTGATCTGT).

RNA seq

For RNA isolation of *in vitro* stimulated T cells, RNeasy mini kit (Qiagen) was used. 200ng of total RNA was used to prepare the library for RNA sequencing. Coexpression patterns of genes associated with effector and memory cell fate, immune checkpoints, effector molecules, and adhesion/homing were chosen based on the literature as depicted in the main text. Data underwent z-score normalization for display as described previously (Xiong et al., 2020). Upstream regulator analysis was performed using Ingenuity pathway analysis software, using a cut-off log2fold change of 1 and a p value of >0,05.

Imaging

Activated T cells were incubated on Poly-L-lysine coated coverslips for 10 min at 37°C and then fixed with 4% PFA for 10min, followed by permeabilization with 0,25% Triton X-100 for 10 mins. Staining for Pgam5 was performed as previously described (Yamaguchi et al., 2019), using rabbit Anti-Pgam5 antibody (ab126534, Abcam). Immune complexes were detected with 1:200-diluted anti-rabbit IgG Alexa Fluor 488 (Thermo Fisher). Nuclei were counterstained with a DAPI-containing liquid mountant (ProLong™ Gold Antifade Mountant, Thermo Fisher). Mitochondria were stained with 200 nM Mitotracker Red for 45min Image were acquired by confocal microscopy.

Histology

For histological analysis of colon tissue, colons were paraffin embedded using the ''swiss roll'' technique and serially sectioned at 200 μm. After deparaffinization and rehydration of the tissue, haematoxylin and eosin (H&E) staining and α-CD3 (IS503: DAKO)

was performed using a Leica Bond Max following standard immunochemistry staining protocols. Stained sections were scanned using Aperio CS2 (Leica). AOM tumor lesion size and incidence were quantified using Aperio ImageScope software.

Protein analysis

$5x10^6$ isolated T cells were stimulated on cell-culture plates coated with 1:200 α-CD3 (145-2C11; 100339; BioLegend) and α-CD28 (37.51; 102115, Biolegend) for the indicated time points. After centrifugation for 5mins at 1500rpm, cell pellets were resuspended in complete protein lysis buffer (50 mM Tris pH 7.5, 250 mM sodium chloride,30 mM EDTA, 25 mM sodium pyrophosphate, 1% Triton-X 100, 0.5% NP-40, 10% glycerol and 1 mM DTT) supplemented with protease and phosphatase inhibitors (Roche). When subcellular location of Pgam5 was studied, a cell fractionation kit (Abcam, Ab109719) was used according to the manufacturer's instructions. Fractionation and whole-cell lysates were snap frozen and stored at -80°C until further analysis. Collected lysates were mixed with 10% β-mercaptoethanol Laemmli buffer and denatured for 10 min at 70°C. Equal amounts of protein as assessed by Bradford measurement (Pierce™ Coomassie Plus (Bradford) Assay Reagent, ThermoFisher) were subjected to 10-15% SDS-PAGE, then transferred to 0.45μM PVDF membranes (MeckMillipore). Membranes were blocked for 30 mins in PBS-T/5% milk or PBST-T/5% BSA prior to antibody incubation overnight with the following antibodies: β-Actin (Sigma; #A4700), Gapdh (Santacruz; sc32233), Parkin (Santacruz; sc32283), Phospho-β-Catenin (CellSignaling; 9561), TOM20 (CellSignaling; D84TN;42406S); pStat1 (Cellsignaling; 9167) and PGAM5 (Abcam; ab126534). Afterwards, membranes were incubated for one hour with their respective HRP-conjugated secondary antibodies (Santacruz: sc2314 and sc2313), followed by development using SuperSignal West Pico Chemoluminescence Substrate (ThermoFischer Scientific). 2D densitometry was perfomed using ImageJ Software (National Institutes of Health, Bethesda, Maryland).

QUANTIFICATION AND STATISTICAL ANALYSIS

All statistical analyses were performed using GraphPad Prism 8. Number of samples and experiments, as well as statistical test used are reported in each figure legend. Sample size was determined by prior experience. Data shown as ±SEM or ±SD according to figure legend. Statistical significance was assessed by the test depicted in the respective figure legend (* $p<0.05$, ** $p<0.01$, *** $p<0.001$ and **** $p<0.0001$).

Immunity, Volume *55*

Supplemental information

Expansion of T memory stem cells with superior anti-tumor immunity by Urolithin A-induced mitophagy

Dominic Denk, Valentina Petrocelli, Claire Conche, Moritz Drachsler, Paul K. Ziegler, Angela Braun, Alena Kress, Adele M. Nicolas, Kathleen Mohs, Christoph Becker, Markus F. Neurath, Henner F. Farin, Christian J. Buchholz, Pénélope A. Andreux, Chris Rinsch, and Florian R. Greten

Figure S1. Urolithin A affects antigen presentation and T cell differentiation, Related to Figure 1

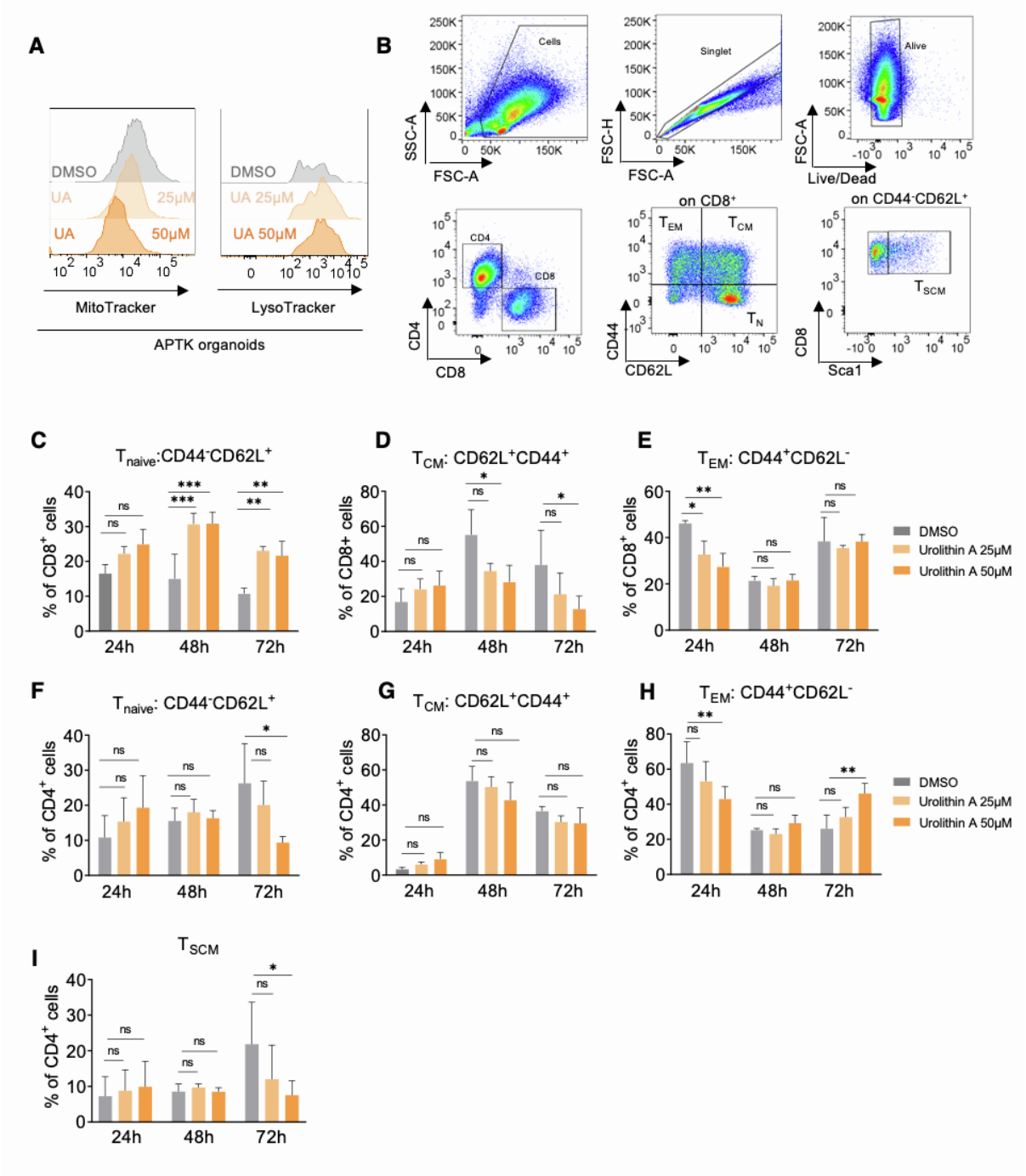

(A) Representative histograms pertaining to Figure 1H-I. Right panel, lysosome formation as assessed by lysotracker MFI via flow cytometry after 24h. Left panel, Mitotracker signal of APTK organoids incubated for 24h at the presence of UA in vitro after 24h incubation at the presence of various UA concentrations. **(B)** Representative gating strategy for identifying naïve

T cell (T_N; $CD44^-CD62L^+$), effector memory cell (T_{EM}; $CD44^-CD62L^-$), central memory cell ($T_{CM;}$ $CD44^+CD62L^+$) and memory stem cell (T_{SCM}; $CD44^+CD62L^+Sca1^+$) subsets within stimulated $CD8^+$ or $CD4^+$T cells. **(C-E)** Quantification of T_N (C), T_{CM} (D) and T_{EM} (E) within $CD8^+$ T cells that were stimulated with αCD3/αCD28 for 48h in the presence of different doses of UA. Data are mean ± SD, n=4, p*<0,05, p**<0,01; ***p <0,001; n.s. not significant by two-way ANOVA followed by Tukey's multiple comparison test. **(F-I)** Complete subset analysis of $CD4^+$ cells, showing the quantification of T_N (F), T_{CM} (G), T_{EM} (H) and T_{SCM} (I) within $CD4^+$ T cells that were stimulated with αCD3/αCD28 for 48h in the presence of different doses of UA. Data are mean ± SD, n=4, p*<0.05, p**<0.01; n.s. not significant by two-way ANOVA followed by Tukey's multiple comparison test.

Figure S2. Urolithin A restricts T cell division, Related to Figure 2

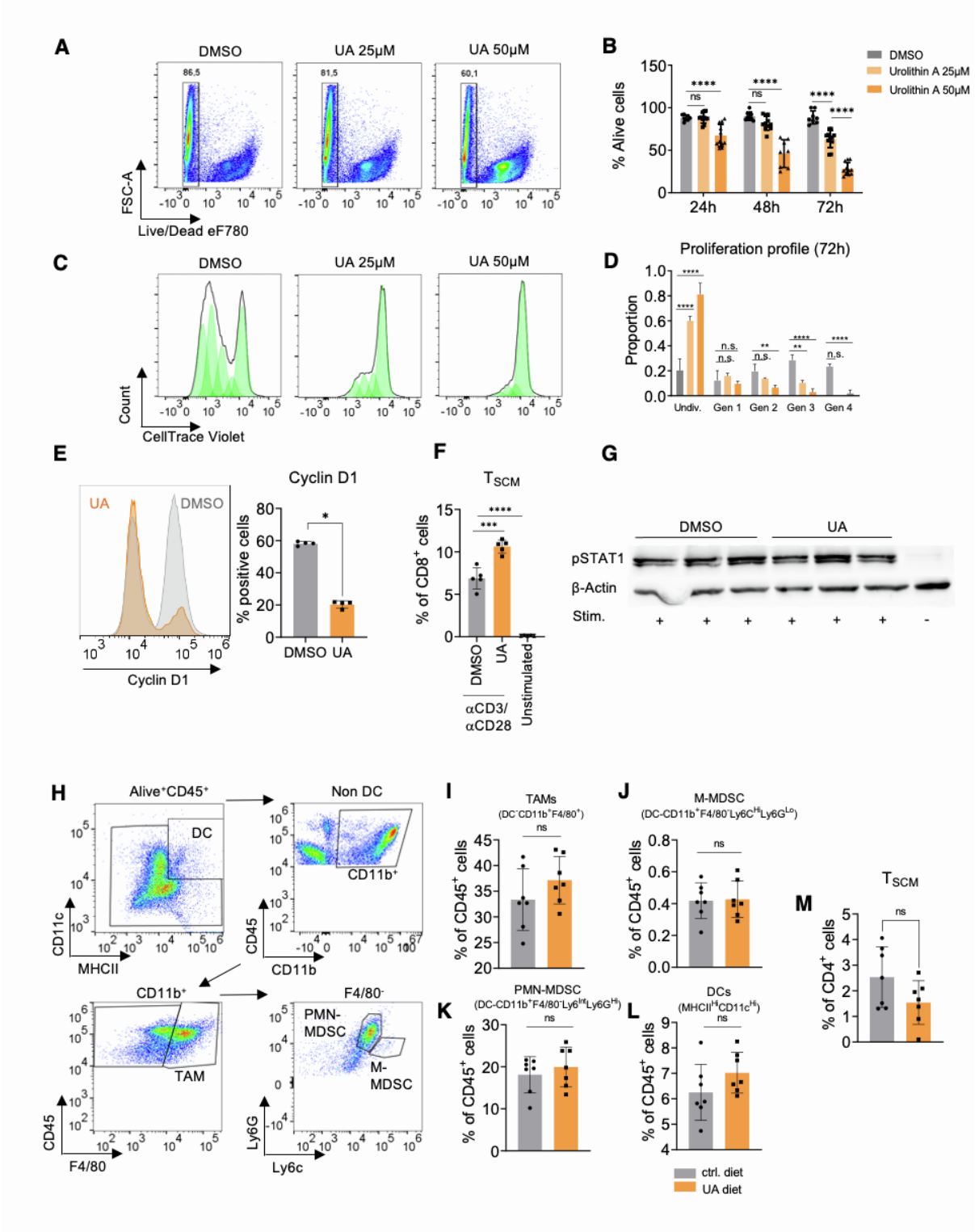

(A) Representative gating strategy for identifying dead cells within murine T cells. **(B)** Analysis of murine CD3+ T cell death upon stimulation at various concentrations of UA at the indicated time points. Data are mean ± SD, n=8-11, ****p <0.0001; n.s. not significant by two-

way ANOVA followed by Tukey's multiple comparison test. **(C-E)** UA restricts T cell proliferation. **(C, D)** Representative analysis of CD8+ T cell proliferation over 72h in response to UA. **(D)** Quantification of proliferation data obtained from (C). Proportion in proliferative generation as assessed via FlowJo Software is shown (Undiv., undivided cells; Gen1, divided once). Data are mean ± SD, n=3, p**<0.01; ****p <0.0001; n.s. not significant by two-way ANOVA followed by Tukey's multiple comparison test. One of two independent experiments is shown. **(E)** Representative analysis of cyclin D1 expression after 48h of αCD3/αCD28 stimulation in the absence of presence of UA (50µM). Data are mean ± SD, n=4, p*<0,05 by two-sided t-test. One of two independent experiments is shown. **(F)** Frequency of T_{SCM} after 48h of αCD3/αCD28 stimulation in the absence or presence of UA (50µM). Data are mean ± SD, n=5/group, ***p <0.001, ****p <0.0001 by one-way ANOVA followed by Tukey's multiple comparison test. **(G)** Immunoblot analysis of T cells stimulated with αCD3/αCD28 for 6h in the absence or presence of UA (50µM). **(H)** Representative gating strategy. **(I-L)** Quantification of **(I)** TAM, **(J)** M-MDSC, **(K)** PMN-MDSC and **(L)** DC in APTK-tumors of mice receiving control or UA-containing diet (treatment regimen in Fig.1K). Data are mean ± SD, n=7/group. Statistical analysis was performed by two-sided t-test. **(M)** Frequency of T_{SCM} within $CD4^+$ TIL of APTK-induced tumors receiving control or UA-containing diet. Data are mean ± SD, n=7, n.s. not significant by two-sided t-test.

Figure S3. OT-1 CD8^{+} phenotype before adoptive T cell transfer, Related to Figure 3

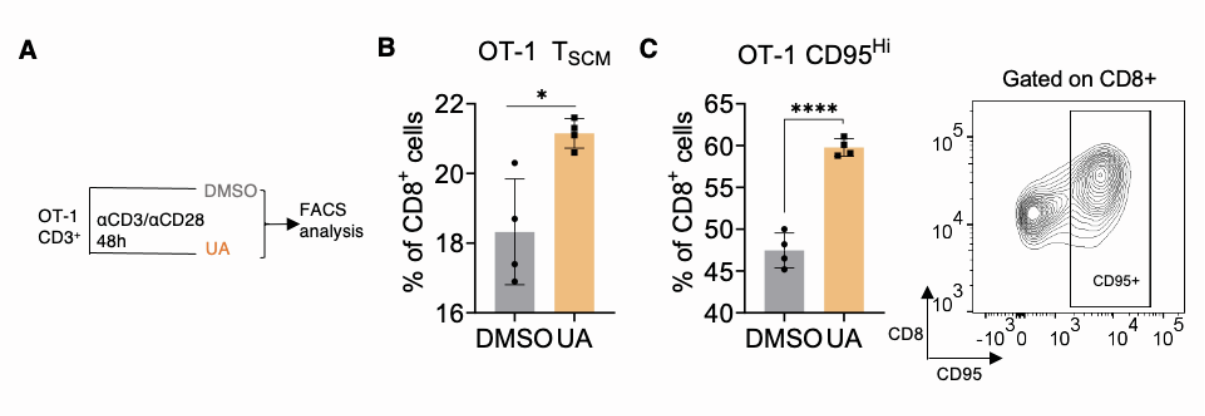

(A) Scheme of OT-1 CD3^{+} T cell activation, treatment, and analysis. **(B)** Quantification of OT-1 CD44^{-}CD62L^{+}Sca1^{Hi} T_{SCM} 48h after αCD3/αCD28 stimulation. Data are mean ± SD, n=4 *p < 0,05, by two-sided t-test. Data from one out of two experiments are shown. **(C)** Quantification and gating strategy of CD95 expression on OT-1 CD8+ cells 48h after αCD3/αCD28 stimulation. Data are mean ± SD, n=4, *****p <0.0001, by two-sided t-test. Data from one out of two experiments are shown.

Figure S4. Activation of Wnt signaling depends on Pink1-mediated mitophagy and subsequent Pgam5 release, Related to Figure 5

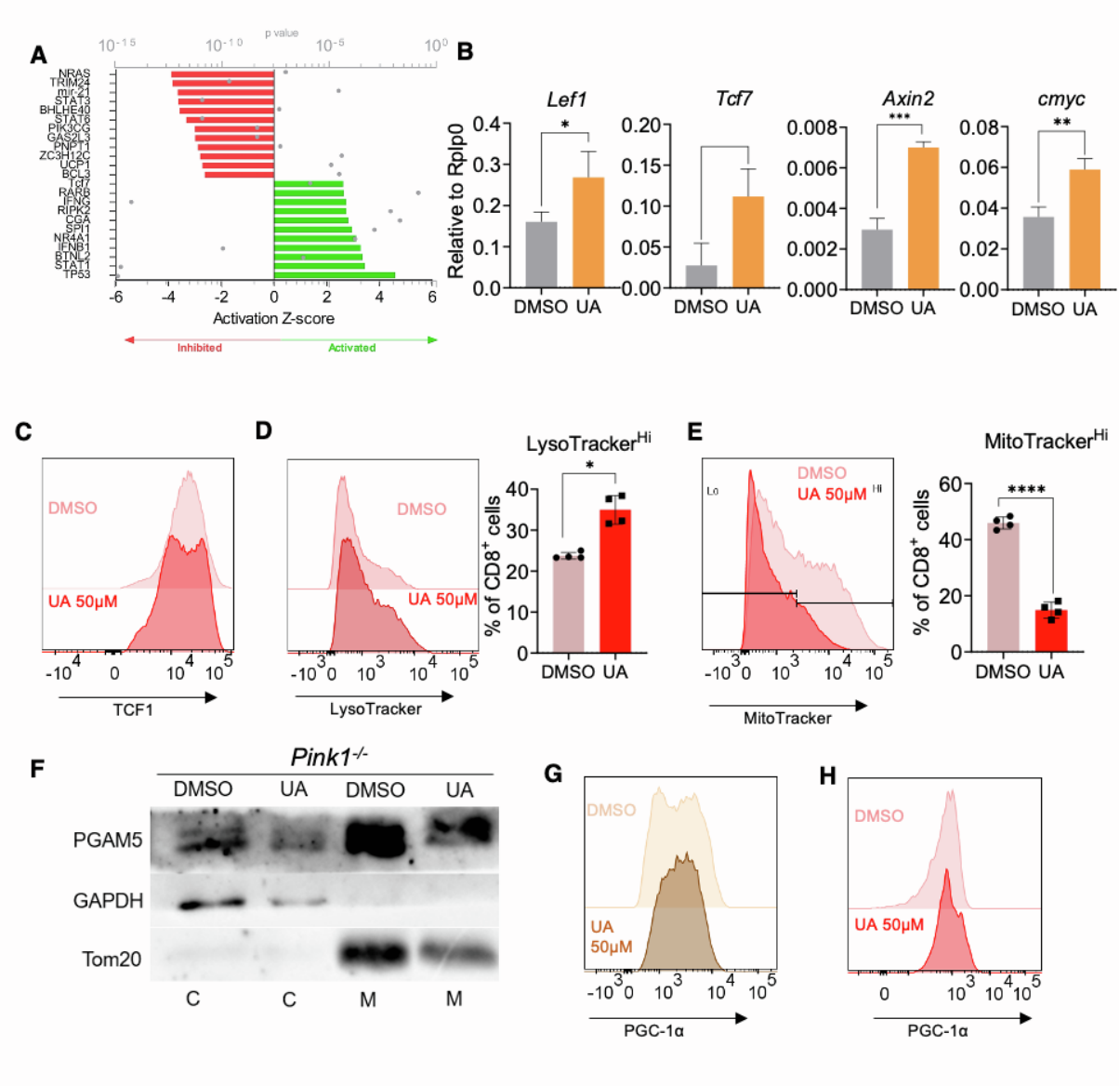

(A) Ingenuity pathway upstream regulator analysis (IPA) of UA-treated T cells. Assessed from RNAseq data. Plausible upregulation is depicted by z score, significance is shown on the overlying dot spot. Genes with a log2 fold change of 1 and $p<0.05$ were initially considered. **(B)** qPCR analysis of selected Wnt target genes 24h after stimulation. Data are mean ± SEM, n=4, *$p<0.05$, **$p<0.01$, ***$p<0.001$ by two-sided t-test. **(C)** Representative histogram for data depicted in Fig. 5K. **(D)** Flow cytometric analysis of lysosome formation in *Pgam5*$^{-/-}$CD8^{+} T-cells after 6h stimulation with αCD3/αCD28 in the absence or presence of UA (50μM), Data

are mean ± SD, * $p<0.05$, by two-sided t-test. **(E)** Mitotracker Red staining after 24h stimulation *Pgam5*$^{-/-}$CD8^{+} T-cells with αCD3/αCD28 in the absence or presence of UA (50μM). Data are mean ± SD, n=4, *** $p<0.001$ by two-sided t-test. **(E)** Immunoblot analysis of cell fractionations of *Pink1*$^{-/-}$ T cells 6h stimulation with αCD3/αCD28 in the absence or presence of UA (50μM). One of two independent experiments is shown (c= cytosolic fraction, m=mitochondrial fraction). **(G-H)** Representative histograms for data depicted in Fig. 5N (G) and Fig. 5M (H).

Figure S5. Identification of human T_{SCM}, Related to Figure 6

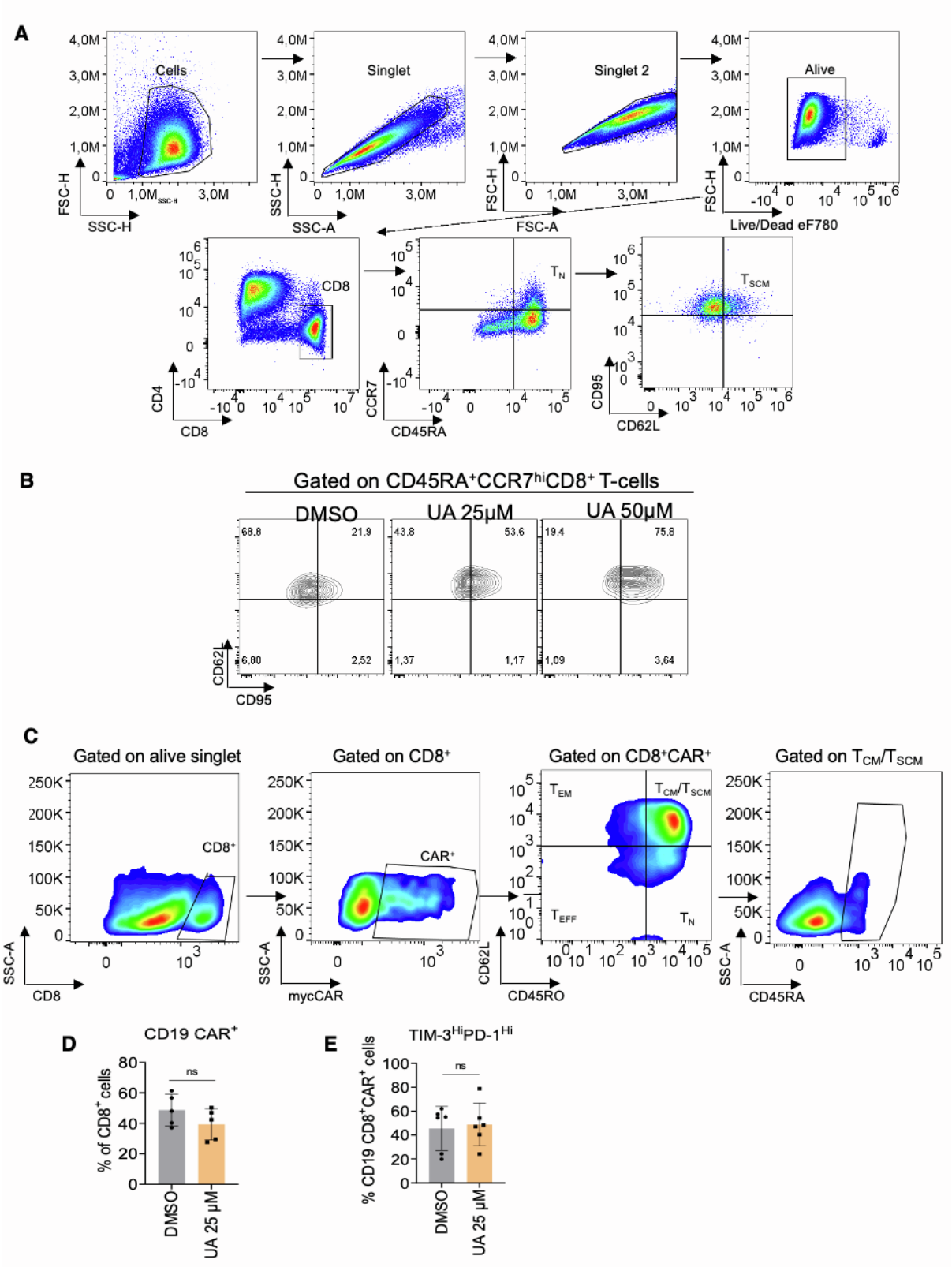

(A) Representative gating strategy for identification of human T_{SCM} ($CD45RA^+CCR7^{Hi}CD62L^+CD95^+CD8^+$). (B) Representative flow cytogram, displaying a

dose-dependent increase of $CD95^{hi}CD62L^{+}$ cells within the $CD45RA^{+}CCR7^{hi}CD8^{+}$ population. **(C)** Representative gating strategy for assessment of CAR expression and identification of human T_{SCM} in CAR T cell experiments. **(D)** Quantification of CD19 CAR-expression on $CD8^{+}$ cells after VSV-LV aided gene transduction at the presence of DMSO or UA (25µM) for 72h. Data are mean ± SD, n=5, n.s. not significant by two-sided t-test. **(E)** Frequency of exhausted $Tim3^{Hi}PD\text{-}1^{Hi}$ $CD8^{+}CAR^{+}$ after activation and CD19 CAR transduction as indicated in Fig. 6E. Data was acquired three days after transduction. Data are mean ± SD, n=6, n.s. not significant by two-sided t-test.

Table S1. List of mouse qRT-PCR primers, Related to STAR Methods

Mouse qRT-PCR Primers		
Atg5	GGAGAGAAGAGGAGCCAGGT	GCTGGGGGACAATGCTAATA
Atg7	GCCTAACACAGATGCTGCAA	TGCTCTTAAACCGAGGCTGT
Atg12	TAAACTGGTGGCCTCGGAAC	ATCCCCATGCCTGGGATTTG
Pik3c3	GTGAAGTACCCTGACCTGCC	AGTCATGCATTCCTTGGCGA
p62	GCTGAAGGAAGCTGCCCTAT	TTGGTCTGTAGGAGCCTGGT
Bnip3	ATGCACAGCATGAGTCGGG	CTGGTATGCATCTCAACATCAAACA
Lamp2	TGTGCAACAAAGAGCAGGTG	TCCAGTATGATGGCGCTTGAG
Pink1	AAGCACCAGAAATTGCGACG	ACGAGATGGGAGTGCTGGTA
Tcf7	CAATCTGCTCATGCCCTACC	CTTGCTTCTGCGTGATGTCC
Rplp0	TTCATTGTGGGAGCAGAC	CAGCAGTTTCTCCAGAGC
Lef1	GCAGCTATCAACCAGATCC	GATGTAGGCAGCTGTCATTC
Axin2	CAGAGGTGGTACCTTGCCAAA	GCCGACAGTGCAAGACCC
cmyc	AACTACGCAGCGCCTCCC	ATTTTCGGTTGTTGCTGATCTGT